Invited Paper:

# The Physical Hydrogeology of Ore Deposits*

S. E. INGEBRITSEN,[1],[†] AND M. S. APPOLD[2]

[1] *U.S. Geological Survey, 345 Middlefield Road, Menlo Park, California 94025*

[2] *Department of Geological Sciences, 101 Geological Sciences Bldg., University of Missouri, Columbia, Missouri 65211*

## Abstract

Hydrothermal ore deposits represent a convergence of fluid flow, thermal energy, and solute flux that is hydrogeologically unusual. From the hydrogeologic perspective, hydrothermal ore deposition represents a complex coupled-flow problem—sufficiently complex that physically rigorous description of the coupled thermal (T), hydraulic (H), mechanical (M), and chemical (C) processes (THMC modeling) continues to challenge our computational ability. Though research into these coupled behaviors has found only a limited subset to be quantitatively tractable, it has yielded valuable insights into the workings of hydrothermal systems in a wide range of geologic environments including sedimentary, metamorphic, and magmatic. Examples of these insights include the quantification of likely driving mechanisms, rates and paths of fluid flow, ore-mineral precipitation mechanisms, longevity of hydrothermal systems, mechanisms by which hydrothermal fluids acquire their temperature and composition, and the controlling influence of permeability and other rock properties on hydrothermal fluid behavior. In this communication we review some of the fundamental theory needed to characterize the physical hydrogeology of hydrothermal systems and discuss how this theory has been applied in studies of Mississippi Valley-type, tabular uranium, porphyry, epithermal, and mid-ocean ridge ore-forming systems. A key limitation in the computational state-of-the-art is the inability to describe fluid flow and transport fully in the many ore systems that show evidence of repeated shear or tensional failure with associated dynamic variations in permeability. However, we discuss global-scale compilations that suggest some numerical constraints on both mean and dynamically enhanced crustal permeability. Principles of physical hydrogeology can be powerful tools for investigating hydrothermal ore formation and are becoming increasingly accessible with ongoing advances in modeling software.

## Introduction

THE PURPOSE of the present communication is to review the application of hydrogeologic principles to the study of hydrothermal ore deposits. Our review consists of three main parts: (1) a presentation of the general theory governing subsurface fluid flow, heat and solute transport, mechanical deformation, and ultimately ore deposition; (2) an exploration of the controlling influence of permeability on the formation of most ore deposits; and finally (3) a generalized hydrogeologic perspective on the origin of selected sedimentary and magmatic hydrothermal deposits. Our focus throughout this communication is mainly on the physical hydrogeology of ore deposits rather than on the geochemistry of ore deposits that is more commonly the focus in economic geology research. We use the term "groundwater" to refer broadly to any subsurface aqueous fluid regardless of its composition, temperature, or geologic setting (Freeze and Cherry, 1979).

In order to create ore deposits, fluids typically must scavenge metals from a large source volume, whether from magma or from rocks encountered along their flow path, and deposit them in a much smaller, downstream volume (Cox, 2005). In the geologic record, this concentrating effect is evident in contrasts of more than three orders of magnitude between calculated fluid/rock ratios in source regions and at deposit sites (Heinrich et al., 2000), and contrasts of about five orders of magnitude between the fluid-volume fluxes inferred for pervasive regional metamorphism ($3 \times 10^{-12}$ m³m⁻²s⁻¹ or m/s; Peacock, 1989) and for midcrustal shear zones (up to $3 \times 10^{-7}$ m/s; Striet and Cox, 1998). Such scavenging and concentration of matter and energy is inherent in many large-scale groundwater-flow systems. In gravity- (i.e., topography-) driven groundwater-flow systems, recharge areas are generally much more extensive than discharge areas (e.g., Tóth, 1963). Discharge can be focused further by permeability contrasts related to faults (e.g., Forster and Smith, 1989) and other discontinuities. The focusing of energy by regional-scale groundwater flow is vividly demonstrated in volcanic

---

terranes, where much of the regional heat flow from areas of 1,000s of km² (100s of MW$_{thermal}$) can be absorbed by groundwater and discharged advectively in a relatively small locus of thermal springs (Manga, 1998; Ingebritsen and Mariner, 2010). Such hydrothermal systems can deposit gold and silver in concentrations of up to three orders of magnitude greater than their average crustal abundances, due largely to the high fluid-flow rates attainable in hot springs, which commonly are on the order of tens of L/s but can reach 1,000 L/s (e.g., Benoit and Butler, 1983; Hochstein and Browne, 2000; Simmons and Brown, 2006). For example, at a volumetric flow rate of 100 L/s and an aqueous gold concentration of only 1 ppb, even the largest gold deposits containing around 1,000 metric tons (t) of gold could be deposited in a few hundred thousand years, which is within the lifespan of order $10^5$ to $10^6$ years considered typical for magmatic hydrothermal systems (Hochstein and Browne, 2000). In other cases, ore formation appears to have been promoted by high metal concentrations in the ore fluid. For example, recent studies show that carbonate-hosted Pb-Zn deposits probably precipitated from brines containing hundreds to thousands of ppm Pb and Zn, much higher than the concentrations typically found in sedimentary brines (Hanor, 1996; Wilkinson et al., 2005, 2009; Huizenga et al., 2006; Piqué et al., 2008; Stoffell et al., 2008; Appold and Wenz, 2011). Such first-order comparisons reveal ore deposits to be hydrogeologically unusual in terms of flow rates, heat content, metal content, or some combination thereof (Fyfe et al., 1978).

The spectrum of ore deposit types found in the Earth's crust is wide, and the formation of most involved a component of fluid flow and advective heat and solute transport. However, in this overview we emphasize ore deposits formed from hydrothermal fluids in subsurface magmatic and sedimentary environments, neglecting skarns, deposits in regionally metamorphosed rocks, deposits related to ultramafic rocks or carbonatites, and deposits related to surficial processes such as weathering (e.g., laterites and bauxites) or precipitation from surface waters (banded iron formation, phosphate, and sedimentary Mn deposits).

## Processes Driving Fluid Flow and Transport

Many economically significant ore deposits are hydrothermal, meaning that they exist because of the transport of solutes and heat by aqueous fluids. This fluid advection can concentrate not only metals but also heat, leading to ore deposit formation temperatures that commonly are significantly higher than expected based on the deposits' formation depth relative to the local background geothermal gradient. Mechanical deformation is also relevant, as many ore deposits show clear evidence of repeated episodes of fracture creation and destruction. Thus, from the hydrogeologic perspective, deposition of ore minerals is a coupled flow problem, and one sufficiently complex that physically rigorous description continues to challenge our computational ability.

Coupled thermal (T), hydraulic (H), mechanical (M), and chemical (C) simulation models are often referred to as THMC models in the context of geothermal reservoir engineering and nuclear-waste isolation, the primary arenas for which the most sophisticated and complete numerical models

have been developed. Although many ore deposits must be regarded as full-fledged THMC systems, the computational state-of-the-art and our limited knowledge of relevant parameters require that quantitative analyses almost invariably neglect some of the relevant couplings.

*Darcy's law and fluid flow*

The conceptual starting point for quantifying subsurface flow and transport is Darcy's law:

$$\mathbf{q}_i = -\frac{\mathbf{k}k_{ri}}{\mu_i}\left(\nabla P_i + \rho_i g \nabla z_g\right). \tag{1}$$

This equation makes it possible to calculate the velocity ($\mathbf{q}_i$) of a fluid phase, $i$, based on knowledge of the intrinsic permeability ($\mathbf{k}$) of the medium through which the fluid is flowing, the relative permeability ($k_{ri}$), which accounts for the reduction in permeability for fluid phase $i$ caused by the presence of other pore fluids, the viscosity ($\mu_i$), density ($\rho_i$), and gradient ($\nabla$) in pressure ($P_i$) of fluid phase $i$, the magnitude of the acceleration due to gravity ($g$), and the gradient in elevation parallel to the direction of gravitational acceleration ($z_g$), where bold typeface is used to denote a vector or matrix quantity. These variables and others introduced later are also defined in the notation section at the end of the manuscript, and typical values of permeability for common geologic media are shown in Figure 1. Equation (1) can be derived theoretically from conservation of momentum (Bear, 1972) and is commonly referred to as the variable-density form of Darcy's law, meaning that the equation is valid for fluids whose density
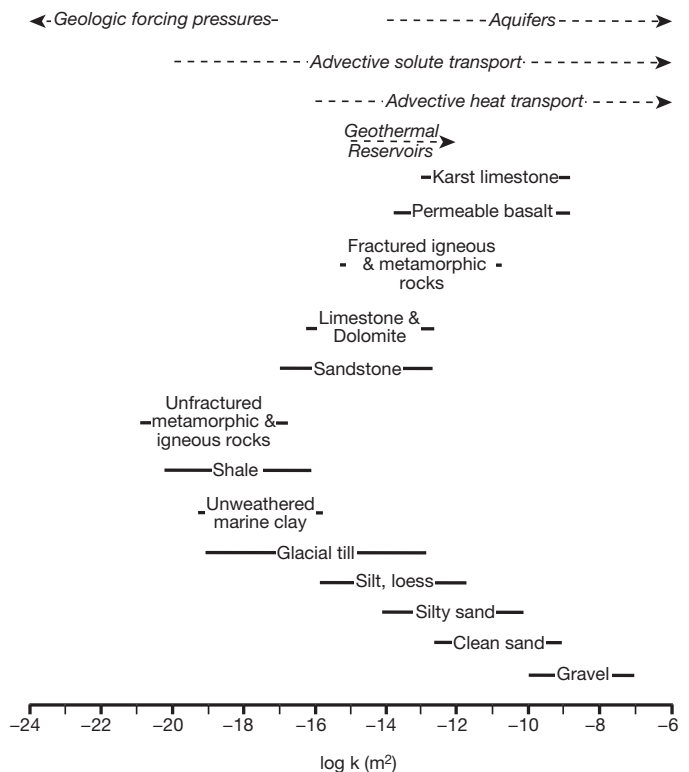


FIG. 1. Range of permeabilities observed in geologic media, showing certain process-limiting values and other selected values discussed in the text. After Freeze and Cherry (1979) and Ingebritsen et al. (2006).

(and for that matter, viscosity) vary spatially within the problem domain. The original, empirically derived form of Darcy's law (Darcy, 1856) is strictly valid only for fluids whose density and viscosity are constant within the problem domain.

Several aspects of equation (1) merit further discussion. The velocity term $\mathbf{q}_i$, a vector, is variably called the Darcy velocity, the Darcy flux, or the specific discharge and represents the volumetric flow rate of fluid per unit total cross-sectional area through which the fluid is flowing. Pore fluid velocity is also expressed as an average linear velocity ($\mathbf{v}_i$) which can be calculated from the Darcy velocity by

$$\mathbf{v}_i = \frac{\mathbf{q}_i}{\phi_e}, \qquad (2)$$

and represents the volumetric flow rate per unit of actual cross-sectional area through which the fluid is flowing. In equation (2), $\phi_e$ is the effective porosity, i.e., the fraction of the total volume of rock that consists of interconnected pores capable of transmitting fluid flow. True microscopic velocities are generally larger than the average linear velocity, because the actual distance traveled by a fluid between two points in the subsurface is typically not the shortest possible distance but a longer, more tortuous path.

The density and viscosity values needed to use equation (1) for pure aqueous fluids and NaCl solutions are available from equations of state reviewed or developed by Haar et al. (1984), Adams and Bachu (2002), Driesner (2007), and Liebscher (2010). The intrinsic permeability ($\mathbf{k}$) is a single value for flow calculated in one spatial dimension, a $2 \times 2$ matrix for flow calculated in two spatial dimensions, and a $3 \times 3$ matrix for flow calculated in three spatial dimensions. Values of the intrinsic permeability vary by at least 15 orders of magnitude as a function of lithology and texture (Fig. 1) and have been compiled in many introductory hydrogeology textbooks, including Freeze and Cherry (1979), Fetter (2001), and Schwartz and Zhang (2003). These references also describe techniques for measuring permeability from flow-rate experiments performed in wells or on drill cores, or the calculation of permeability from porosity or grain-size distributions. The relative permeability ($k_{ri}$) is a fraction that varies from 0 when fluid phase $i$ occupies none of the available pore space to 1 when fluid phase $i$ saturates (occupies all of) the available pore space. Relative permeability functions are typically determined empirically for specific rock media and pore fluid combinations. For aqueous liquid-vapor systems, the Corey (1954) functions have been found to work particularly well (Horne et al., 2000).

When one of the coordinate axes in the problem domain is parallel to the direction of gravitational acceleration (vertical), then equation (1) simplifies to the following widely cited equation:

$$\mathbf{q}_i = - \frac{\mathbf{k}k_{ri}}{\mu_i} (\nabla P_i \pm \rho_i \mathbf{g}). \qquad (3)$$

where $\mathbf{g}$ is the gravitational acceleration vector (not just the magnitude of the vector as in eq 1) and the terms inside the parentheses are added if the vertical coordinate represents depth and subtracted if the vertical coordinate represents elevation.

To calculate the pressure gradient ($\nabla P_i$) of fluid phase $i$, the remaining term needed to apply Darcy's law, the spatial distribution of fluid pressure and its variation in time must be known. In some modern fluid-flow systems, pressure can be measured in the field. In most cases, however, the pressure must be calculated. This can be done for any fluid phase $i$ that either partially or fully occupies the available pore space, using

$$\frac{\partial(\phi S_i \rho_i)}{\partial t} = \nabla \cdot \left[ \frac{\mathbf{k}k_{ri}\rho_i}{\mu_i} (\nabla P_i + \rho_i g \nabla z_g) \right] + R_m, \qquad (4)$$

where $\phi$ is the total or overall porosity, $S_i$ is the fraction of the total pore volume occupied by fluid phase $i$, $R_m$ represents a source or sink of fluid phase $i$, and $t$ is time. Equation (4) is a statement of conservation of mass in which the change in fluid mass over time in an arbitrary volume (left term) is equal to the net mass flux that crosses the volume (first term on the right) plus the rate of fluid mass production inside the volume. In the context of dynamically evolving hydrothermal systems, the source/sink term $R_m$ can represent fluids produced by processes such as release of magmatic volatiles, metamorphic devolatilization, or hydrocarbon production, or fluids consumed by hydration reactions.

The term on the left side of equation (4) can be expanded to

$$\frac{\partial(\phi S_i \rho_i)}{\partial t} = (c_u + \phi \beta_i) \rho_i S_i \frac{\partial P_i}{\partial t} + \phi \rho_i \frac{\partial S_i}{\partial P_c} \frac{\partial P_c}{\partial t}, \qquad (5)$$

where $c_u$ is the uniaxial compressibility of the rock medium, $\beta_i$ is the compressibility of fluid phase $i$, and $P_c$ is capillary pressure. Compressibility values of common geologic media are shown in Table 1. Compressibility values for liquid and vapor can be determined as partial derivatives of the equations of state for density. The first term on the right side of equation (5) expresses the loss or gain of fluid due to compaction or expansion of the medium and pore fluid as a result of fluid pressure changes. The second term on the right side of equation (5) reflects loss or gain of fluid due to changes in capillary pressure, which arises when two or more fluids occupy a pore, creating attractive forces at the interface of the fluids and the solid matrix. It follows that when only one fluid is present there is no capillary pressure and the second term on the right side of equation (5) becomes zero. When liquid

TABLE 1. Coefficient of Compressibility for Common Geologic Media

| Material | Compressibility ($Pa^{-1}$) |
|---|---|
| Plastic clay | $2.6 \times 10^{-7} - 2 \times 10^{-6}$ |
| Stiff clay | $1.3 \times 10^{-7} - 2.6 \times 10^{-7}$ |
| Medium-hard clay | $6.9 \times 10^{-8} - 1.3 \times 10^{-7}$ |
| Loose sand | $5.2 \times 10^{-8} - 1 \times 10^{-7}$ |
| Dense sand | $1.3 \times 10^{-8} - 2 \times 10^{-8}$ |
| Dense, sandy gravel | $5.2 \times 10^{-9} - 1 \times 10^{-8}$ |
| Fissured rock | $3.3 \times 10^{-10} - 6.9 \times 10^{-10}$ |
| Sound rock | $<3.3 \times 10^{-10}$ |
| Limestone | $1.5 \times 10^{-11} - 4.2 \times 10^{-11}$ |
| Dolomite | $6.7 \times 10^{-12} - 4.8 \times 10^{-11}$ |
| Sandstone | $2.0 \times 10^{-11} - 2.4 \times 10^{-10}$ |
| Shale | $2.6 \times 10^{-11} - 2.4 \times 10^{-10}$ |
| Granite | $2.1 \times 10^{-11} - 4.5 \times 10^{-11}$ |
| Diorite | $1.5 \times 10^{-11} - 2.5 \times 10^{-11}$ |
| Basalt | $1.9 \times 10^{-11} - 3.0 \times 10^{-11}$ |
| Gabbro | $1.8 \times 10^{-11} - 3.5 \times 10^{-11}$ |
| Marble | $1.5 \times 10^{-11} - 6.0 \times 10^{-11}$ |
| Gneiss | $2.5 \times 10^{-11} - 5.3 \times 10^{-11}$ |

Sources: Domenico and Mifflin (1965); Henderson and Henderson (2009)

water and its vapor are the pore fluids, the capillary pressure is defined as

$$P_c = P_v - P_l, \tag{6}$$

where $P_v$ is the pressure of the aqueous vapor and $P_l$ is the pressure of the aqueous liquid. Thus, in order to solve the governing equation (4) for the pressure of fluid phase $i$ in a multiphase fluid system, the relationship between the saturation of fluid phase $i$ and capillary pressure must be known or estimated so that $\partial S_i / \partial P_c$ can be evaluated.

*Heat transport*

Heat transport in a hydrothermal system consisting of aqueous liquid and vapor can be evaluated using the following conservation of energy equation:

$$\frac{\partial [\phi \rho_f H_f + (1 - \phi) \rho_r H_r]}{\partial t} = \\ -\nabla \cdot (\rho_v \mathbf{q}_v H_v) - \nabla \cdot (\rho_l \mathbf{q}_l H_l) - \nabla \cdot (K_m \nabla T) + R_h, \tag{7}$$

where $H$ is enthalpy, $K_m$ is thermal conductivity of the bulk-rock medium, $T$ is temperature, $R_h$ is a heat source or sink, and the subscripts, $l$, $v$, $f$, and $r$ designate aqueous liquid, aqueous vapor, bulk fluid (liquid and vapor), and the rock matrix, respectively. The value of $K_m$ can be found from

$$K_m = K_r^{(1 - \phi)} K_f^{\phi}, \tag{8}$$

where $K_r$ and $K_f$ represent the thermal conductivity of the rock matrix and pore fluid, respectively. Values of $K_m$ are shown in Table 2 and are temperature dependent (e.g., Sass et al., 1992).

Equation (7) states that the amount of heat that accumulates or diminishes within an arbitrary volume (left term) is balanced by the net flux of heat transported through the volume by vapor (first term on right side), liquid (second term on right side), and conduction (third term on right side), and by the amount of heat produced or consumed within the volume. The heat-source ($R_h$) term can be used to represent local endothermic or exothermic processes such as crystallization.

TABLE 2. Thermal Conductivity Values for
Common Geologic Media at 20°C

| Material | Thermal conductivity, $K_m$ (W m⁻¹ K⁻¹) |
|---|---|
| Claystone and siltstone | 0.80–1.25 |
| Shale | 1.05–1.45 |
| Sand | 1.70–2.50 |
| Sandstone | 2.50–4.20 |
| Quartzite | 4.20–6.30 |
| Lithic sand | 1.25–2.10 |
| Graywacke | 2.70–3.35 |
| Limestone | 2.50–3.10 |
| Dolomite | 3.75–6.30 |
| Salt | 4.80–6.05 |
| Anhydrite | 4.90–5.80 |
| Coal | <0.5 |
| Water | 0.59 |
| Granite | 2.50–3.35 |
| Basalt and andesite | 1.45–2.10 |
| Rhyolite glass | 1.25–1.45 |
| Rhyolite ash | 0.60–1.05 |
| Rhyolite welded tuff | 1.70–2.10 |

Source: Blackwell and Steele (1989)

Equation (7) is posed in terms of enthalpy to provide a convenient way of dealing with latent heat of vaporization (Faust and Mercer, 1979), which is the difference between liquid ($H_l$) and vapor ($H_v$) enthalpies). Although the pressure-entropy pair has certain advantages in representing very high velocity flows (Lu and Kieffer, 2009), that approach has not yet been implemented in published numerical simulators. Use of temperature as the single dependent variable, though perhaps a more intuitive choice, results in a less general heat transport equation because the pressure-temperature combination does not uniquely specify the proportions of vapor and liquid. For example, for a pure-water system at atmospheric pressure, the single pressure-temperature combination of 0.1 MPa (1 bar) and 100°C applies to vapor-liquid proportions ranging from entirely liquid to entirely vapor and, as a result, to large ranges in bulk fluid density (0.6–987 kg/m³) and enthalpy (418–2,676 kJ/kg), respectively (Fig. 2).

Although four different enthalpy terms ($H_f$, $H_r$, $H_v$, $H_l$) and temperature ($T$) appear in equation (7), the only dependent
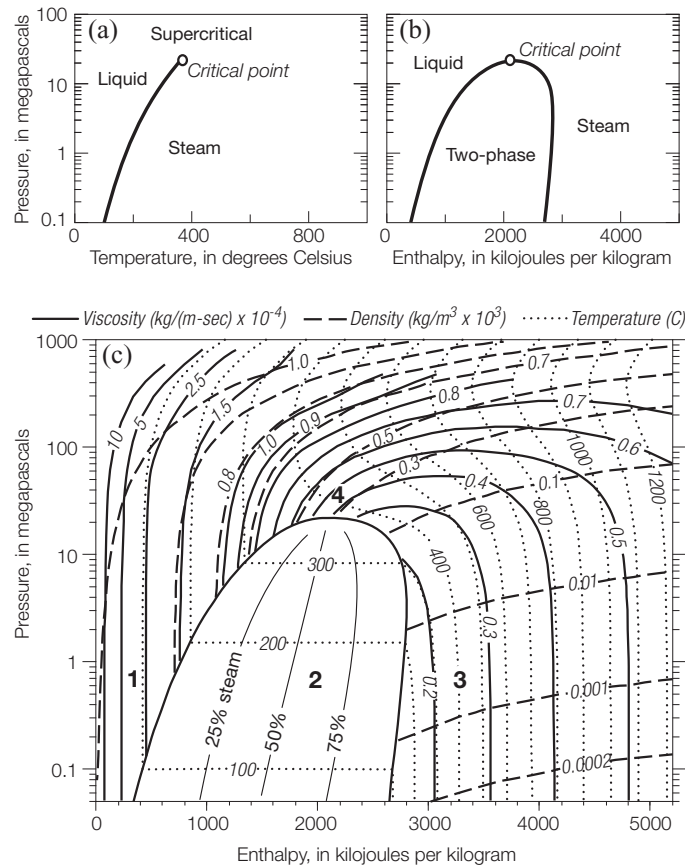


FIG. 2. (a). Pressure-temperature and (b) pressure-enthalpy diagrams, showing thermodynamic regions; (c) pressure-enthalpy diagram showing contours of equal temperature, density, viscosity, and mass fraction steam. In (b) and (c) the curves bounding the two-phase region define the enthalpies of saturated steam and liquid water; they intersect at the critical point (22.055 MPa and 2086 kJ/kg). In (c), the thermodynamic regions are denoted by (1) "compressed" liquid water, (2) two-phase, (3) superheated steam, and (4) supercritical fluid. On a microscopic scale, any particular water molecule will lie either on the saturation curves or fully outside the two-phase region. However, on the macroscopic scale at which we model hydrogeologic systems, some model elements may contain a mixture of phases, and these will lie in the two-phase region.

variable is the enthalpy of the bulk fluid $H_f$. When the hydrothermal fluid consists of only one phase, then the enthalpy of the bulk fluid equals the enthalpy of the fluid phase present (e.g., $H_f = H_l$) and $T$ is a unique function of $H_f$ and fluid pressure $P$. When both liquid and vapor are present, then values of $P$ determined from equation (4) uniquely specify both temperature and the enthalpies of the liquid and vapor (Fig. 2). In most hydrothermal settings, except where fluid-flow rates are very high as in geysers or phreatic eruptions, local thermal equilibrium exists between the rock matrix and fluid phases, meaning that the rock and fluids have the same temperature. Given the heat capacity ($c_r$) of the rock, the rock enthalpy ($H_r$) can be computed from temperature via the definition for heat capacity at constant pressure

$$c_r = \frac{dH_r}{dT}. \qquad (9)$$

Equation (7) is coupled to fluid flow via the groundwater velocity term ($\mathbf{q}$) that appears there and in Darcy's law, equations (1) and (3). Additional coupling between fluid flow and heat transport occurs through the enthalpy- and pressure-dependent fluid density and viscosity terms, which appear not only in equations (1), (3), and (7) but also in equation (4), which is used to calculate the fluid pressure fields that help drive fluid flow. The couplings are nonlinear because coefficients that are functions of both dependent variables (e.g., $\rho_v$) are multiplied by the dependent variables.

*Solute transport*

The transport of a solute component, $j$, by a flowing fluid phase, $i$, can be described by the following mass conservation equation:

$$\frac{\partial(\phi \rho_i S_i C_j)}{\partial t} = \nabla \cdot (\phi_e \rho_i \mathbf{v}_i C_j) + \nabla \cdot (S_i \phi_e \rho_i \mathbf{D} \nabla C_j) + R_j, \quad (10)$$

where $C_j$ represents the mass concentration of solute component $j$ and $\mathbf{D}$ represents the dispersion coefficient tensor. The term on the left side of equation (10) represents the rate of solute mass accumulation in an arbitrary volume of porous rock, the first term on the right side of the equation represents solute transport by fluid advection, the second term on the right side of the equation represents solute transport by dispersion, and the third term, $R_j$, represents a source or sink of the solute component. The components of the dispersion coefficient can be calculated from

$$D_{ij} = \alpha_{ijkl} \frac{v_k v_l}{|v|} + \frac{D_w}{\tau}, \, i, j, k, l = 1, \dots n_d, \qquad (11)$$

where $\alpha$ is the dispersivity of the porous medium and represents its tendency to disperse or dilute solute due to pore-scale velocity variations, $D_w$ is the solute diffusion coefficient in open water, $\tau$ is the tortuosity of the interconnected pore space, $|v|$ is the magnitude of the average linear velocity, and $n_d$ is the number of spatial dimensions. Like the dispersion coefficient, the dispersivity is a tensor. In practice, the dispersivity is commonly reduced to a three-term matrix consisting of a longitudinal component parallel to the direction of flow ($\alpha_L$) and two transverse components orthogonal to the direction of flow, one in the vertical direction ($\alpha_{TV}$) and one in the horizontal direction ($\alpha_{TH}$; Burnett and Frind, 1987).

Longitudinal dispersivity values are a function not only of the properties of the rock but also of the scale of measurement and have been reviewed and compiled by Schulze-Makuch (2005). Transverse dispersivities are typically less than or equal to longitudinal dispersivities. Ratios of longitudinal to transverse dispersivity of order 100 have been reported from relatively homogeneous aquifers and the ratios typically decrease with increasing heterogeneity.

Kinetic rate expressions that affect the concentration of $j$ can be substituted for $R_j$. If reactions are treated as reaching local equilibrium, then mass-action expressions (e.g., $K_{eq} = \prod \alpha_j^{ej}$) would be computed in tandem with equation (10) at each time step. Laboratory experiments (e.g., Seyfried, 1987; Bischoff and Rosenbauer, 1988, 1996; Bischoff et al., 1996; Foustoukos and Seyfried, 2007), observations of geothermal spring, sea-floor vent, and volcanic fumarole compositions (e.g., Giggenbach, 1984; Von Damm, 1990, 1995; Shinohara, 2008), and thermodynamic calculations (e.g., Reed and Spycher, 1984; Symonds et al., 2001) show that circulating hydrothermal fluids are highly reactive, which causes strong feedback effects in the fluid-flow field. These feedbacks arise because mineral precipitation and dissolution reactions alter porosity and permeability, which alters fluid velocity, which alters heat and solute transport, which in turn affects the density and viscosity of the fluid and the progress of chemical reactions. Reactive solute-transport simulations of hydrothermal systems require a tremendous amount of computational power, in part because the fluid must be speciated at each time step and an equation (10) must be calculated for every solute component. Thus simulations have mainly been limited to one- or two-dimensional domains with relatively simple geometries.

*Mechanical deformation*

Mechanical deformation in elastic rocks subjected to changes in fluid pressure and temperature can be described by

$$G\nabla^2 \mathbf{u} + \frac{G}{1-2v} \nabla (\nabla \cdot \mathbf{u}) = \alpha_e \nabla \hat{P} + G \frac{2(1+v)}{1-2v} \alpha_T \nabla \hat{T}, \quad (12)$$

where the circumflex (ˆ) above $P$ and $T$ is used to indicate an increase or decrease, rather than an absolute value, $\mathbf{u}$ is the displacement vector, $\alpha_e$ is the effective stress coefficient, $\alpha_T$ is the medium thermal expansivity, and $G$ is the shear modulus, the ratio of the shear stress to shear strain. This equation essentially relates strain (or deformation)—on the left side of the equation—to the stresses imposed by changes in pressure and temperature. The individual terms in equation (12) do not readily lend themselves to concise, intuitive definition; we refer interested readers to Neuzil (2003), Wang (2000), or Ingebritsen et al. (2006, p. 39–61) for full discussion and developments. Calculated pressure changes (from eq 4) and temperature changes (from eq 7) can be inserted into equation (12) to obtain the strain and the displacements experienced by a porous rock matrix. Strain also affects fluid pressure and permeability and thus, to represent poroelastic behavior fully, equation (12) must be coupled with a fluid pressure equation that incorporates a volumetric strain term (which eq 4 lacks). In this context, "coupling" means that the equations are linked by incorporating the same strains and fluid pressures in their mathematical solutions. Problems in

porothermoelasticity require coupling with equations of heat transport (such as eq 7) as well.

The theory of "linear poroelasticity" represented by equation (12) represents the current state-of-the-art of hydrogeologic modeling. This state-of-the-art is inadequate to describe fluid flow fully in the many ore deposits such as porphyry and epithermal deposits that show evidence of repeated shear and tensional failure with associated dynamic changes in permeability. The theory of coupled flow, transport and inelastic deformation is still under development.

### Numerical solution

Systems of coupled equations such as equations (1), (4), (7), (10), and (12) are amenable to analytical solution—direct integration of the partial differential equations—in only a few very specialized cases. In general they must be solved by numerical methods that transform the partial differential equations into systems of algebraic equations that are conceptually easier but computationally more laborious than analytical methods. For numerical solution, the physical domain is represented by a computational grid consisting of a number of discrete points located on the intersection of lines that are orthogonal to each other ("structured grid") or in a nonorthogonal arrangement that can optimize the representation of geometrical features within the domain ("unstructured grid"). The number of grid points feasible or desirable in practical applications depends greatly on factors such as the computational efficiency of the numerical method and the complexity of the geologic structures to be represented. At each grid point, values of the parameters that describe the physical domain—for example, porosity and permeability—are specified from field or laboratory determinations, or assumed and subsequently tested and varied during sensitivity analysis. Once parameter values have been assigned, the governing equations are approximated numerically at each grid point. A number of documented, open-source algorithms are now available to solve systems of transport equations like those described above (Table 3).

## The Controlling Influence of Permeability

*"The mantra of hydrogeologists and … ore deposits geologists alike is 'permeability, permeability, permeability'…"* (Richards and Tosdal, 2001)

TABLE 3.  Relative Capabilities of Selected Multiphase Numerical Codes Commonly Applied in Simulations of High-Temperature Hydrothermal Systems

| Name[1] (Reference) | $T_{max}$ (°C) | $P_{max}$ (MPa) | Numerical method[2] | Reactive transport | Deformation | $CO_2$[3] | $X_{NaCl}$[3] |
|---|---|---|---|---|---|---|---|
| CSMP++ (Matthäi et al., 2007; Coumou, 2008) | 1,000 | 500 | FE-FV | | | | X |
| FEHM (Zyvoloski et al., 1988, 1997; Bower and Zyvoloski, 1997; Dutrow et al., 2001; Keating et al., 2002) | 1,500 | | FE | X | X | X | |
| FISHES[4] (Lewis, 2007; Lewis and Lowell, 2009) | 800 | 1,000 | FV | | | | X |
| HYDROTHERM (Hayba and Ingebritsen, 1994; Kipp et al., 2008) | 1,200 | 1,000 | FD | | | | |
| NaCl-TOUGH2 (Kissling, 2005) | 620 | 100 | IFD | | | | X |
| TOUGH2 (Pruess, 1991; Pruess et al., 1999) | 350 | 100 | IFD | | | X | X |
| TOUGH2-BIOT (Hurwitz et al., 2007) | 350 | 100 | IFD-FE | | X | X | |
| TOUGH-FLAC (Rutqvist et al., 2002) | 350 | 100 | IFD-FE | | X | X | |
| TOUGHREACT (Xu et al., 2004) | 350 | 100 | IFD | X | | X | |

[1] Interactive websites:
    CSMP++ <http://csmp.ese.imperial.ac.uk/wiki/Home>
    FEHM <http://fehm.lanl.gov/>
    HYDROTHERM <http://wwwbrr.cr.usgs.gov/projects/GW_Solute/hydrotherm/>
    TOUGH2 <http://esd.lbl.gov/TOUGH2/>
[2] Numerical methods: FD = finite difference, IFD = integrated finite difference, FE = finite element, FE-FV = finite element-finite volume
[3] The columns labeled $CO_2$ and $X_{NaCl}$ indicate whether the EOS formulations include those components
[4] Successor model to GTHM (Lowell and Xu, 2000; Bai et al., 2003)

*Role of permeability in solute and heat transport*

It is evident from Darcy's law (eqs 1, 3) that the rate at which fluids flow through geologic media is strongly controlled by permeability. Thus, permeability directly affects the rates of advective solute and heat transport and therefore the potential for ore genesis. At sufficiently low permeabilities, solute transport occurs mainly by diffusion (contained within the dispersion coefficient in the second term on the right side of eq 10), and heat transport occurs mainly by the analogous process of heat conduction (third term on the right side of eq 7). Diffusion and conduction do not depend directly on the rate of fluid flow, but except at very low flow rates, their contributions to solute and heat transport are small compared to the advective contribution by the flowing fluid. The effectiveness of advective solute transport (first term on the right side of eq 10) is proportional to the average linear pore velocity, **v**. Analytical solutions for one-dimensional flow and transport (cf. Finlayson, 1992) show that advection will substantially affect the concentration distribution for Darcy velocities of $q \geq 10^{-13}$ m/s, assuming a length scale of a few hundred meters and that $\phi \sim 0.1$. By invoking Darcy's law and further assuming a hydraulic gradient less than or equal to unity ($dh/dL < 1$), we can equate this flow rate to a hydraulic conductivity of $>10^{-13}$ m/s. For liquid-water density $\rho_l$ and viscosity $\mu_l$ at 15°C, this value of hydraulic conductivity translates to an intrinsic permeability of $k \sim >10^{-20}$ m² (Fig. 1). The effectiveness of advective heat transport (first and second terms on the right side of eq 7) is proportional to the quantity $c_f \rho_f q$, where $c_f$ is the heat capacity of the fluid. Analytical solutions show that, over a similar length scale, advection of heat by liquid water can begin to affect the temperature distribution substantially at flow rates on the order of $10^{-9}$ m/s (Bredehoeft and Papadopulos, 1965). For $dh/dL < 1$, this translates to hydraulic conductivities $\geq 10^{-9}$ m/s or permeabilities of $k \sim \geq 10^{-16}$ m² (Fig. 1). The roughly $10^4$ difference between the permeability thresholds for advection-dominated solute transport and advection-dominated heat transport is due to the relative efficiency of conduction as a heat-transport mechanism versus diffusion as a solute-transport mechanism (Bickle and McKenzie, 1987).

In most ore-forming environments both solute and heat transport are dominated by advection, at least episodically, so that we can infer $k \sim \geq 10^{-16}$ m². More likely, permeabilities associated with most ore deposits are at least $k \sim 10^{-15}$ m², which is the minimum value for commercially viable geothermal reservoirs (Fig. 1) and has also been shown to be the optimal value of bulk permeability for generating hot and potentially vapor-rich hydrothermal plumes (Hayba and Ingebritsen, 1997; Driesner and Geiger, 2007). The most permeable rocks widely exposed at the Earth's surface are young, unaltered basalt flows, with a log $k$ (m²) typically –13 to –9 (Fig. 1).

*Effect of permeability on fluid pressure*

Low permeabilities can also be process limiting. When permeabilities are sufficiently low, the fluids generated or released by such processes as subsidence and sedimentation, petroleum generation, pressure solution, crustal deformation, and mineral dehydration can significantly influence fluid pressures. These phenomena can all be expressed in equation

(4), either in terms of compression or expansion of the medium (on the left side of eq 4) or addition of fluid (the $R_m$ term on the right side of eq 4). Fluid release (or sequestration) by various geologic processes can have a very large effect on fluid pressures when moderately large regions of a flow domain ($L > 100$ m) are composed of or bounded by material with log $k$ (m²) $\sim \leq -17$ (based on $|\Gamma_d| > 1$, where $\Gamma_d$ is $[R_m L]/[\rho_f K]$ and $K$ is the hydraulic conductivity, $k \rho_f g / \mu_f$; Neuzil, 1995; Fig. 1). Many ore deposits record evidence of episodically high fluid pressures and thus log $k \sim \leq -17$, at least episodically (e.g., Jowett, 1987; Henley and Hughes, 2000; Sibson, 2001; Gruen et al., 2010). The least permeable rocks widely exposed at the Earth's surface are marine shales, which commonly act as aquitards or confining layers to maintain high fluid pressures (log $k$ typically –21 to –19, Fig. 1).

*Anisotropy in permeability*

Throughout this discussion of permeability we have ignored its directional dependence (anisotropy) and for the most part will continue to do so, although permeability in the general case is regarded as a second-order tensor (eqs 1, 3, 4). Anisotropy is typically imparted by rock fabric, such as sedimentary or volcanic bedding, jointing and fracturing, or metamorphic foliation. Anisotropy can be characterized by measuring permeability in the direction of the rock fabric and in the directions orthogonal to the rock fabric. Permeability of rock samples (e.g., drill core) can be measured in the laboratory by applying a known pressure gradient across the sample and determining the flow rate of fluid through the rock, though such measurements commonly underestimate the larger scale permeability of hydrogeologic units. Various field methods for measuring permeability have been devised (e.g., pump tests in groundwater withdrawal wells and slug and packer tests in monitoring wells or well bores; U.S. Bureau of Reclamation, 2001) whose results are valid over larger scales (10s to 100s m) but typically assume permeability to be isotropic. Geochemical proxies for permeability, such as water/rock ratios typically offer little information about anisotropy as they tend to reflect the primary orientation of flow. Thus, anisotropy can be difficult to constrain accurately, particularly for paleoflow systems such as those that form ore deposits.

*Permeability-depth relationships*

Global-scale compilations suggest some possible constraints on numerical values of permeability. Geothermal data and estimates of fluid flux during prograde metamorphism have been used to constrain the mean permeability of the continental crust (Fig. 3). A power-law fit to these data yields a geothermal-metamorphic permeability-depth curve,

$$\log k \approx -14 - 3.2 \log z, \quad (13)$$

where $k$ is in m² and $z$ is in km (Manning and Ingebritsen, 1999). The geothermal data represent 0 to 10 km depth and come from a variety of tectonic settings, including sedimentary basins, volcanic terranes, and crystalline bedrock. The metamorphic data represent 6 to 30 km depth in regions undergoing active metamorphism and tectonism (i.e., orogenic belts). The empirical fit to this data (eq 13; Fig. 3a, blue curve) defines a value of log $k$ (m²) at 1 km depth (–14) that is equivalent to Brace's (1980) mean in situ permeability of
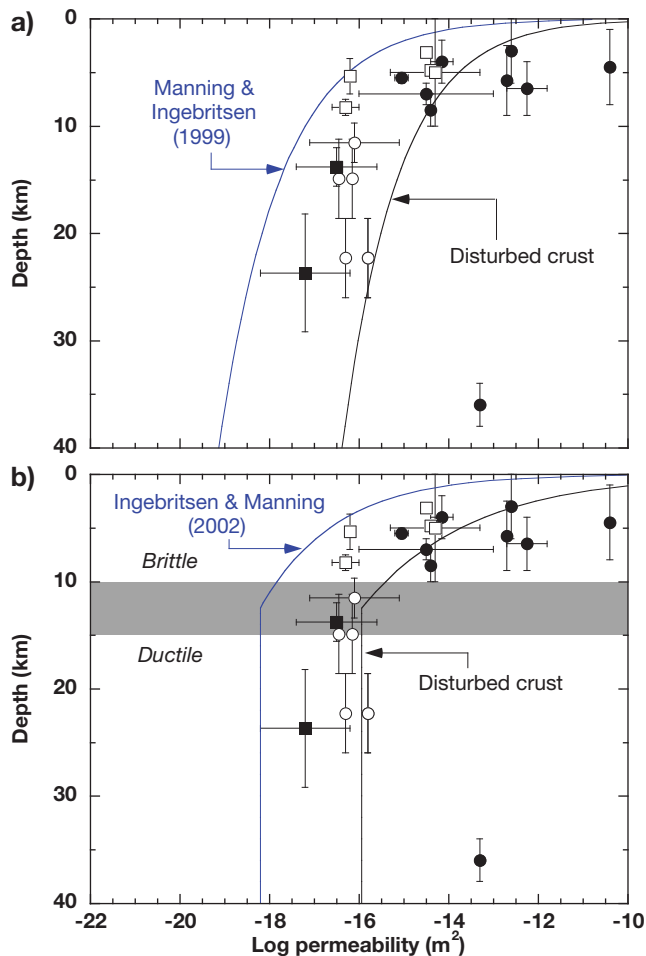
FIG. 3.  Solid blue curves represent the mean permeability of tectonically active crust and are based on coupled models of groundwater flow and heat transport fitted to geothermal observations (0–10 km depth) and site-specific estimates of metamorphic fluid flux (6–30 km depth; Manning and Ingebritsen, 1999; Ingebritsen and Manning, 2002). Solid black curves are fitted to permeability data for disturbed crust: rapid migration of seismic hypocenters (solid circles); enhanced rates of metamorphic reaction in major fault or shear zones (open circles); recent studies suggesting much more rapid metamorphism than had been canonically assumed (solid squares); and anthropogenic disturbance (RMA, enhanced geothermal systems; open squares). After Ingebritsen and Manning (2010): (a). Power-law fit to data (eqs 13, 14). (b). Data below 12.5 km depth fitted with constant values of $10^{-18.3}$ m² (blue curve) and $10^{-16.0}$ m² (black curve). After Ingebritsen and Manning (2010).

crystalline rocks. Below a depth of about 10 to 15 km, the base of the brittle-ductile transition zone in most tectonically active crust (Ruff, 2004), permeability effectively remains constant at about $\log k \approx -18.3$ (Fig. 3b, blue curve). The values of $k$ from metamorphic systems likely reflect the maximum principal component of the permeability tensor, which in many cases seems to be subhorizontal (e.g., Ferry, 1992). A modest degree of anisotropy ($k_z/k_x \sim 1/10$) would permit fluid pressures in the deeper crust to be near lithostatic (e.g., Fyfe et al., 1978) for the average metamorphic $q$ value of $\sim 10^{-11}$ m/s (Ingebritsen and Manning, 1999). Townend and Zoback (2000) found equation (13) to be compatible with data from in situ hydraulic tests and from seismicity induced either by fluid injection or reservoir impoundment, and equation (13)

has since been used successfully in modeling crustal-scale fluid flow (Lyubetskaya and Ague, 2009) and shown to be reasonably compatible with other independently compiled data (Shmonov et al., 2002, 2003; Saar and Manga, 2004; Stober and Bucher, 2007).

## The dynamic nature of permeability

Many economic geologists, geophysicists, and metamorphic petrologists have long recognized permeability as a dynamic parameter that changes in response to tectonic stress, dewatering and fluid production, and other geochemical reactions (e.g., Sibson et al., 1975; Walder and Nur, 1984; Yardley, 1986; Sibson, 1987; Titley, 1990; Hanson, 1992, 1995, 1997; Rice, 1992; Dutrow and Norton, 1995; Connolly, 1997; Cox, 2002; Sibson and Rowland, 2003; Yardley and Baumgartner, 2007). This view is in stark contrast to the traditional hydrogeologic concept of permeability as a relatively static material property that exerts control on fluid flow. However, a growing body of observational evidence suggests that the permeability of the brittle upper crust may be dynamically self adjusting, responding to tectonic stress (e.g., Townend and Zoback, 2000) and external fluid sources (Rojstaczer et al., 2008), much as the lower crust responds to the magnitude of internal fluid sources (e.g., Fyfe et al., 1978). This evidence seems compatible with the concept of "dynamic permeability" (Cathles and Adams, 2005).

Substantial evidence exists for local-to-regional-scale, transient, permeability-generation events that require permeabilities much higher than the mean $k$-$z$ relationships such as equation (13) would suggest (Ingebritsen and Manning, 2010). Compilation of such data from disturbed, seismically active crust yields a best fit of

$$\log k \approx -11.5 - 3.2 \log z, \qquad (14)$$

suggesting a similar functional form, but shifted to higher permeability at a given depth (Fig. 3a). Both the original geothermal-metamorphic data set (eq 13; Fig. 3a, blue curve) and the disturbed crust data set (eq 14; Fig. 3a, black curve) suggest high variance and strong depth dependence of permeability at crustal depths of less than 10 to 15 km, with less variance and essentially no depth dependence below 10 to 15 km depth, the approximate depth of the brittle-ductile transition. This supports a general distinction between the hydrodynamics of a brittle upper crust and a ductile lower crust that is dominated by devolatilization reactions and internally derived fluids. Both data sets can reasonably be fitted with a constant value of $\log k$ below 12.5 km depth, with an offset of about two orders of magnitude ($\log k$ (m²) $\sim -18.3$ vs. $\log k$ $\sim -16.0$). Although the disturbed crust values in Figure 3 may be ephemeral in the context of geologic time, they can be crucially important from the standpoint of heat and mass transport.

Data from deep boreholes around the world have gradually elucidated the relationship between fluid pressure, stress, and permeability in the brittle upper crust (Raleigh et al., 1976; Hsieh and Bredehoeft, 1981; Barton et al., 1995; Townend and Zoback, 2000). These data indicate that most hydraulically conductive fractures are critically stressed (very near the point of failure) under the existing state-of-stress (Fig. 4). This in turn implies that any small increase in fluid
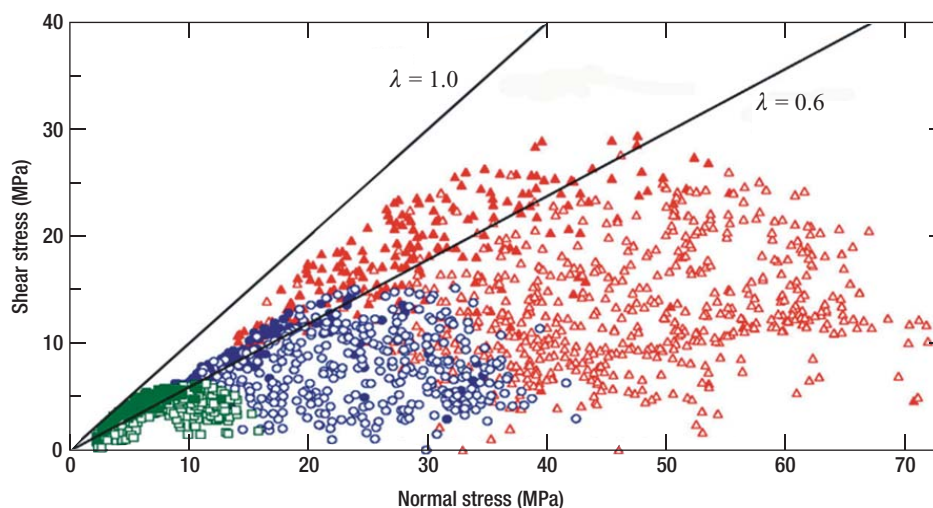
FIG. 4. Shear and normal stresses on individual fractures in three deep boreholes in the western United States. Filled symbols are hydraulically conductive fractures; open symbols are nonconductive fractures. The diagonal lines represent Coulomb failure criteria for coefficients of friction ($\lambda$) of 0.6 and 1.0 and assuming negligible cohesive shear resistance. Thus most of the conductive fractures are in a state of incipient failure, given a coefficient of friction of 0.6 or greater ($\lambda$ is the tangent of the angle of internal friction, which is commonly ~30°). The nonconductive fractures are generally not in a state of incipient failure. Red triangles = Cajon Pass, blue circles = Long Valley, green squares = Nevada test site. After Townend and Zoback (2000).

pressure can trigger failure on (and increase the permeability of) appropriately oriented fractures.

How much pressure (or stress) change might trigger seismicity and enhance permeability? Data from the Rocky Mountain Arsenal indicate that fluid injection-induced failure occurred there at relatively low fluid pressures (Hsieh and Bredehoeft, 1981). The initial fluid pressure in the injection zone was ~27 MPa at 3.6 km depth. The pressure increase required to trigger failure was only about 3 MPa, implying that the Precambrian gneiss beneath the Denver basin was failing when fluid pressures were still subhydrostatic relative to the land surface. Thus high absolute values of fluid pressure are not required for failure. Both the Rocky Mountain Arsenal example and the borehole data compiled in Figure 4 suggest that small pressure (stress) changes can trigger failure even when pressures are near hydrostatic.

The causal pressure (stress) change may sometimes be much smaller than the value of 3 MPa documented at the Rocky Mountain Arsenal. A growing number of cases have been documented in which seasonal variations in seismicity are attributed to hydrologic effects (Wolf et al., 1997; Ohtake and Nakahara, 1999; Heki, 2001, 2003; Saar and Manga, 2004; Christiansen et al., 2005, 2007; Hainzl et al., 2006; Bollinger et al., 2007; Bettinelli et al., 2008), as well as many well-documented cases of seismicity induced by dams and subsequent reservoir impoundment (Talwani et al., 2007). Some of these observations suggest shear failure in response to stress changes on the order of $10^{-1}$ MPa or less. Presumably any finite shear offset would have some finite effect on permeability.

Many hydrothermal veins appear to record numerous pulses of rapid hydrothermal flow ($k \geq 10^{-15}$ m$^2$) interspersed with episodes of much slower flow that may indicate permeabilities sufficiently low to allow substantial fluid-pressure increases ($k \sim \leq 10^{-17}$ m$^2$). The offset permeability-depth curves in Figure 3 suggest a semiquantitative perspective on such behavior.

Permeability may perhaps be viewed as cycling between mean conditions (blue curves) and disturbed-crust conditions (black curves). The similar form of the mean and disturbed crust curves may reflect a confining pressure-dependence of porosity-strain and permeability-strain relationship (Cox, 2002, fig. 1). However, even the disturbed-crust values of Figure 3 may underestimate the maximum transient permeabilities. In prograde metamorphism and sedimentary diagenesis, for instance, fluid generation can be an intermittent process. Produced fluid may migrate through the crust as high porosity and permeability waves (Connolly, 1997; Appold and Nunn, 2002). Resolving full cycles of transient permeability build-up and decay has so far been difficult, as geochemical or thermal alteration signatures produced along the flow paths represent time-integrated fluid fluxes and average permeabilities, though some four-dimensional seismic studies have yielded promising results (e.g., Haney et al., 2005).

*Implementation of permeability in THMC models*

Economic geologists have long recognized that the quantity named "intrinsic permeability" by hydrogeologists is in fact a dynamic parameter. This understanding is nicely summarized by Cox (2005, p. 39):

"… elevated temperature, elevated confining pressure, and the presence of reactive pore fluids typically drive rapid destruction of permeability in fractured and porous rock. Ongoing deformation is required to regenerate permeability and facilitate the high fluid flux necessary to produce hydrothermal ore deposits. A dominant influence is provided by … stress states, fluid pressures, and reactions that … compete with permeability destruction… Devolatilization reactions in prograding metamorphic systems play a key role in generating transitory elevated permeability in deep crustal reservoirs… Below the [brittle-ductile] transition, steady-state-creep

processes favor near-constant permeabilities and continuous fluid flow. In the seismogenic [brittle] regime, large changes in … permeability during the seismic cycle produce episodic flow… To achieve the necessary time-integrated fluid fluxes [for ore deposits] requires redistribution of fluid … during numerous rupture cycles…"

However, such sophisticated conceptual understanding is difficult to implement fully in quantitative THMC models such as those represented by the governing equations discussed in the previous section on "Processes Driving Fluid Flow and Transport." Solution of these equations requires actual numerical values of permeability (and other material properties) to be specified at every grid point within a network that represents the physical domain. Recent quantitative work on dynamic permeability represents an initial attempt to model (Rojstaczer et al., 2008) and parameterize (Ingebritsen and Manning, 2010) this sophisticated conceptual model, but it is not yet possible to model the dynamic evolution of permeability over many orders of magnitude in a satisfactory way. Current quantitative models of hydrologic-mechanical coupling (i.e., permeability creation) typically invoke either single or multiple continua (with, for instance, linear poroelasticity; eq 12) or single, discrete fractures. Only recently have Earth scientists begun to simulate multiple, interacting fractures (Paluszny and Matthai, 2009) and their hydraulic consequences (Paluszny and Matthai, 2010). Modeling of hydrologic-chemical coupling and its hydraulic consequences (mainly permeability destruction through mineral precipitation) is hampered by inadequate knowledge of the properties of complex fluids (e.g., $\rho$ and $\mu$ and their partial derivatives), incomplete reaction-rate and thermodynamic data for many reactions of interest, and ambiguity regarding the appropriate porosity-permeability relationships (Lu and Kieffer, 2009; Ingebritsen et al., 2010). However, ongoing investments in geologic carbon sequestration and geothermal energy (e.g., Fairley et al., 2010) are driving sustained efforts to understand and model permeability evolution better.

The current state-of-the-art representation of permeability enhancement by inelastic strain is embodied in the shear-dilation model (Willis-Richards et al., 1996; Rahman et al., 2002; Kohl and Megel, 2007), which can be written

$$k^{1/3} \propto \alpha = \frac{\alpha_0 + U_s\tan(\Phi_{\mathrm{dil}})}{1 + 9\sigma_{\mathrm{eff}}/\sigma_{\mathrm{nref}}}, \qquad (15)$$

where $\alpha$ is the total fracture aperture after dilation, $\alpha_0$ is the initial aperture, $U_s$ is shear displacement, $\Phi_{\mathrm{dil}}$ is the shear dilation angle, $\sigma_{\mathrm{eff}}$ is the effective normal stress, and $\sigma_{\mathrm{nref}}$ is effective normal stress to a fracture. This model applies to a known distribution of idealized (penny-shaped) cracks—mapped or stochastically generated—and assumes Mohr-Coulomb-style failure and that the cubic law for permeability applies; that is, fracture permeability $k = Nd^3/12$ where $N$ is fracture spacing and $d$ is fracture aperture (Snow, 1968). Most of the independent variables in equation (15) are poorly constrained, and model validation is limited.

### Permeability and earthquakes

A growing body of evidence indicates that the dynamic strain (strong ground motion) associated with distant earthquakes can significantly enhance permeability (Rojstaczer et al., 1995; Sato et al., 2000; Elkhoury et al., 2006; Manga and Rowland, 2009). A seismic energy density of ~ >$10^{-1}$ J/m$^2$ can enhance permeability by up to a factor of ~15 (Wang and Manga, 2010), though this enhancement is unlikely to be great enough to promote ore deposition in rocks that were not already relatively permeable. Much greater permeability enhancement and therefore potential for ore formation is possible proximal to earthquakes, where intensive shear or tensional failure can occur, particularly in locations where earthquakes are recurrent. This explains the well-known association of ore deposits with faults.

Many ore deposits are associated specifically with fault jogs and tips rather than the principal, throughgoing portions of faults, for which at least two explanations are possible (Micklethwaite et al., 2010): (1) large offsets (mainshocks) on well-developed, throughgoing faults may not generate much permeability because the fault core consists of ductile material with an initially low ($k$ = $10^{-22}$ to $10^{-18}$ m$^2$; Morrow et al., 1984) and hard-to-increase permeability; (2) mainshocks on the main fault do in fact generate substantial permeability, but it is short-lived, and recurrence intervals are large; thus numerous aftershocks near fault jogs and tips (Fig. 5) maintain permeability more effectively. During the lifetime of a large, active fault system, aftershock domains localized by large fault jogs may be reactivated thousands of times (Sibson, 2001; Cox, 2005; Micklethwaite et al., 2010). In strike-slip environments, jogs promote vertical connectivity (e.g., Cox, 2005) whereas in normal- or reverse-fault environments, jogs have subhorizontal plunges. In either case, they must tap metal-fertile reservoirs to become mineralized.

It is clear that permeability can be enhanced by sufficiently low effective stress (sufficiently high fluid pressure). One model that provides a reasonable fit to data from the upper few kilometers of the crust is

$$k = k_0\exp(-\sigma_{\mathrm{eff}}/\sigma^*), \qquad (16)$$

where $k_0$ is a reference permeability, $\sigma_{\mathrm{eff}}$ is the effective normal stress ($\sigma - P$), and $\sigma^*$ is an empirical constant (Rice, 1992). Fault-valve models that invoke fluid-pressure-driven permeability enhancement have been applied to mesothermal ($\geq 200°$–$300°$C) and epithermal gold systems (Sibson et al., 1988; Willis and Tosdal, 1992) and entail sudden permeability enhancement by fault rupture that opens connections between deeper, metal-fertile high-pressure reservoirs and shallower, low-pressure reservoirs. The 1997 $M_w$ 5-6 Umbria-Marche thirty-day earthquake sequence (Miller et al., 2004) and the 2009 $M_w$ 6.3 L'Aquila, Italy earthquake (Lucente et al., 2010; Terakawa et al., 2010) may be emblematic of fault-valve behavior. A subducting carbonate platform provides a continuous supply of deeply derived $CO_2$ to Italy west of the Apennines, where diffuse degassing is observed over large regions. High fluid pressures at depth were postulated in the case of the Umbria-Marche sequence (Miller et al., 2004) and also appear to have contributed to the 2009 L'Aquila earthquake (Savage, 2010). Assuming that seismic slip on optimally oriented faults occurs under hydrostatic fluid pressures (Fig. 4), overpressured reservoirs ($\leq 40$ MPa excess pressure) are inferred to occur at 7.5 to 10 km depth in the L'Aquila region and correspond closely to earthquake hypocenters (Terakawa et al., 2010). An abrupt change in the elastic properties of
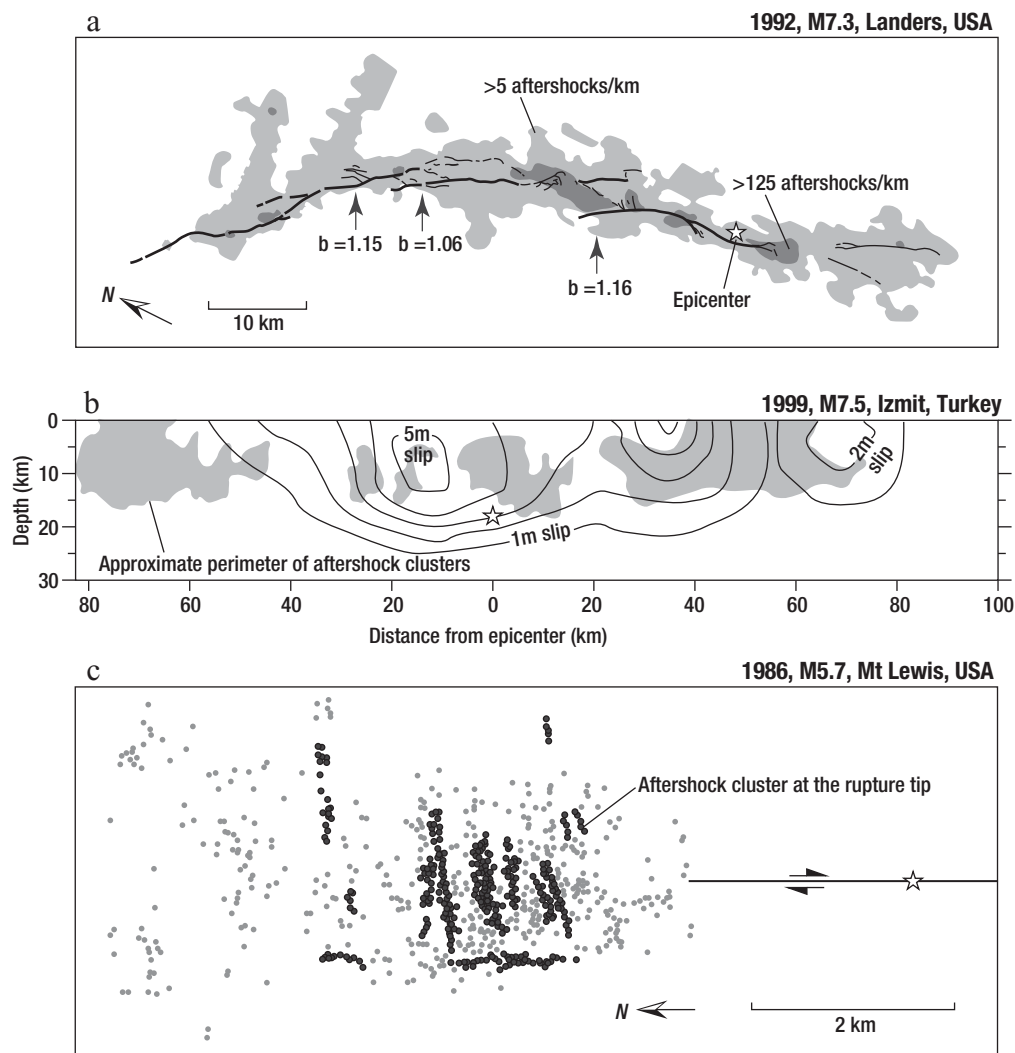
FIG. 5. (a). Map of the Landers, California, earthquake surface-rupture trace, showing areas of high aftershock density and frequency (b values >1) correlated with step-overs and bends. (b). Along fault cross section of the Izmit, Turkey, slip distribution, showing areas of high aftershock density (shading) concentrated along the perimeter of the mainshock rupture plane (contours). (c). Map of Fort Lewis, Idaho, aftershocks, showing aftershocks clustered near the tip of the mainshock rupture and aligned on linear trends, indicating multiple reactivation of individual fault planes (dark symbols). Stars in (a) and (b) are epicenter and hypocenter locations, respectively. From Micklethwaite et al. (2010).

rocks in the fault region (the ratio between compressional- and shear-wave velocity, $V_p/V_s$), coincident with the largest foreshock ($M_w$ 4.0) near L'Aquila, was attributed to breaking of a seal between hanging wall and footwall and subsequent redistribution of fluids (Lucente et al., 2010).

### Ore Deposits in Sedimentary Settings

Many sediment-hosted deposits such as Mississippi Valley-type (MVT) lead-zinc deposits, sediment-hosted massive sulfide (SMS) deposits, and tabular uranium deposits formed in the absence of significant local, concurrent mechanical deformation. Thus, paleohydrologic reconstructions based on systems of fluid flow and heat- and solute-transport equations such as equations (1), (4), (7), and (10) can be regarded as physically rigorous and have provided valuable genetic insights over the past several decades. In the ensuing discussion we focus on ore deposits that formed in sedimentary basins generally in the absence of concurrent igneous activity, emphasizing MVT deposits in particular. The magmatic-hydrothermal deposits discussed in the subsequent section entail additional complexities and challenges.

Most hydrothermal ore deposits form in highly permeable rocks (Misra, 2000). This high permeability may be a dynamic feature of the rocks, for example, in areas of active magmatism and/or faulting where permeability can increase and subside episodically, or a static feature of the rocks, for example, in aquifers that have a high intrinsic permeability and are not subjected to major thermal or mechanical stresses.

#### *Mississippi Valley-type (MVT) deposits*

Mississippi Valley-type deposits typically occur as stratabound mineralization in permeable platform carbonate rocks or, more rarely, sandstones (Leach and Sangster, 1993; Leach et al., 2010). The most common ore minerals include sphalerite

(ZnS), galena (PbS), barite ($BaSO_4$), and fluorite ($CaF_2$). MVT deposits occur worldwide, but those of the United States midcontinent have historically been the most productive and are the best studied. As recently as the mid-1970s, a single ore district in Southeast Missouri, the Viburnum Trend, accounted for 15% of world and 85% of United States lead production (Vineyard, 1977), though the district's relative productivity has now fallen to about 2.7% of world and 26% of United States lead production (U.S. Geological Survey, 2011). The United States midcontinent MVT deposits appear to have formed from brines that migrated laterally for hundreds of kilometers (Bethke and Marshak, 1990; Garven et al., 1993; Appold and Garven, 1999; Appold and Nunn, 2005). Paleomagnetic dating (Wu and Beales, 1981; Wisniowiecki et al., 1983; Pan et al., 1990; Symons and Sangster, 1991; Symons et al., 2005) and radiometric dating (Brannon et al., 1996a, b; Coveney et al., 2000) indicate that the deposits formed mainly during large compressional tectonic events.

Many lines of evidence point to the importance of regional-scale fluid flow in MVT genesis; uniformity of sphalerite banding (McLimans et al., 1980) and cathodoluminescent banding (e.g., Rowan, 1986) in samples across distances of 10s to 100s of kilometers, regionally coherent lead isotope patterns (Heyl et al., 1966; Goldhaber et al., 1995), regional-scale chemical resetting of paleomagnetic pole positions (McCabe and Elmore, 1989), the involvement of mineralizing brines derived from distant basins (Garven, 1985; Leach, 1994), and the deposits' anomalously high formation temperatures of 80° to 150°C at inferred shallow formation depths of <2 km (e.g., Beaumont et al., 1987; Pelch, 2011; Wenz et al., 2012), in contrast with typical continental temperature gradients of 20° to 35°C/km (e.g., Jessop, 1990). Principles of physical hydrology discussed in the preceding sections have played a valuable role in evaluating driving mechanisms and paths of fluid flow, characterizing the temperature and salinity evolution of mineralizing fluids, and constraining the time available for mineralization.

The formation of large, sediment-hosted Pb-Zn (and Cu-Pb-Zn) deposits likely requires the mineralizing fluids to have been able to travel through highly permeable confined aquifers (Cathles and Adams, 2005). In the United States midcontinent this can be seen from the fact that all of the major MVT deposits and likely ore-fluid travel paths are in aquifers that were probably separated from the paleoground surface by intervening regional aquitards (e.g., Jolly and Heyl, 1964; Grogan and Bradbury, 1968; Heyl, 1968; Gaylord, 1995; Appold and Garven, 1999). Such confinement by overlying low-permeability units would promote the long-distance transport of heated groundwater by inhibiting mixing and isolating deeper flow systems from the perturbing effects of local topography, which tend to interrupt and short-circuit regional flow paths (Freeze and Witherspoon, 1967; Garven, 1989).

Groundwater temperatures significantly higher than the conductive temperature gradient generally require permeability heterogeneity (Forster and Smith, 1989; Hurwitz et al., 2003). Groundwater systems with uniformly high permeability are effectively cooled by fluid advection, with the important exception of hydrothermal plumes driven by large and shallow, localized magmatic heat input (such as at midocean ridges: Jupp and Schultz, 2000; Coumou et al., 2008).

By contrast, in systems with uniformly low permeabilities, temperatures follow the conductive geothermal gradient as the advective heat transport contribution will be low (see eq 7).

Confinement is one common and important form of permeability heterogeneity, and particularly relevant to MVT and other stratabound base metal deposits. A simple criterion for effective confinement is

$$\frac{b}{L} << \frac{k_{\text{con}}}{k_{\text{aq}}}, \tag{17}$$

where $b$ is confining-layer thickness, $L$ is aquifer length, and $k_{\text{aq}}$ and $k_{\text{con}}$ are permeabilities of the aquifer and confining layer, respectively (Phillips, 2009, p. 100–105). For the great aquifer systems of the midcontinent of the United States, $b$ is on the order of 100s of m, $L$ is on the order of 100s of km, and $\log k_{\text{aq}}$ and $\log k_{\text{con}}$ ($m^2$) are approximately –12 (Gleeson et al., 2011) and –16 to –20 (Neuzil, 1994), respectively, meaning that the regional-scale aquifer systems are effectively confined.

The MVT deposits of the central United States have been the subject of many paleohydrogeologic reconstructions. Extensive TH, THM, and THC modeling has explored several genetic hypotheses (Sharp, 1978; Bethke, 1985; Garven et al., 1993; Arnold et al., 1996; Garven and Raffensperger, 1997; Appold and Garven, 1999, 2000; Nunn and Lin, 2002; Appold and Nunn, 2005).

The hypothesis that mineralizing brines were driven upward and toward basin margins by vertical loading and/or tectonic compression (e.g., Oliver, 1986) has been generally dismissed, because numerical modeling indicates that the rates of fluid flow from steadily compacting basins would be too small to explain the thermal observations (Cathles and Smith, 1983; Bethke, 1985). In a purely compaction-driven flow regime, flow rates would be sufficient only to raise near-surface temperatures in relatively small discharge areas, whereas fluid inclusion data indicate anomalous temperatures on a regional scale (e.g., Coveney et al., 1987; Ragan et al., 1996). Compaction-driven flow of pore waters originally stored in the sediments constitutes a finite source of fluids that seems unable to deliver sufficient heat (Bethke, 1985) and may (Cathles and Adams, 2005) or may not (Ge and Garven, 1992) provide sufficient brine volume.

For gravity-(topography-) driven flow models, the availability of fluid is limited only by the likely recharge rates and aquifer permeabilities, and by the longevity of the flow system; such models are much better able to explain the thermal observations than the compaction-driven flow models (e.g., Garven and Freeze, 1984a, b; Bethke and Marshak, 1990; Garven et al., 1993). Required fluid-flow velocities are large, typically on the order of at least meters per year (Garven and Freeze, 1984b; Appold and Garven, 1999), but perhaps not unreasonably so in light of the likely high permeability ($k \geq 10^{-12}$ $m^2$) of the regional aquifers of the United States midcontinent during the time of MVT ore formation.

Elevated temperatures in topography-driven flow regimes require high permeability not only in the ore-fluid aquifer, but also high permeabilities ($k > 10^{-13}$ $m^2$) in the recharge zone (Garven, 1984b; Deming and Nunn, 1991; Appold and Garven, 1999; Nunn and Lin, 2002; Appold and Nunn, 2005). If permeabilities were significantly lower, then groundwater

temperatures near the shallower basin margins, where many MVT deposits occur, would not reach the 100° to 150°C window recorded by fluid inclusions unless regional heat flow was anomalously high ($\geq$80 mW/m²), thermal conductivity of one or more stratigraphic units above the deposits was very low (e.g., because of high organic shale or coal content, or high porosity), or MVT deposit formation depths were significantly greater than has previously been estimated. Topography-driven flow systems in which permeabilities are high enough to allow advective heat transport to perturb the conductive geothermal gradient also tend to flush saline fluids from sedimentary basins with dilute meteoric water in relatively short periods of time, on the order of a few million years or less. This therefore leaves a similarly short window of time during which flow rate, temperature, and salinity could have simultaneously been high enough for MVT deposit formation.

These relationships prompted Deming (1992) to propose an alternative model involving convection in crystalline basement rock underlying the sedimentary strata (Fig. 6). Enhanced basement permeability induced by the orogenic event itself allows convection cells to develop; heat and metals leached by the convection cells feed into an overlying gravity-driven flow system. Convection in the basement was assumed to be an inherently episodic process that might account for the rhythmically banded nature of some MVT deposits. This alternative model has yet to be fully explored via THMC modeling, in part because it raises the issue of inelastic deformation and associated dynamic variations in permeability, for which a fully satisfactory theory has yet to be developed. Convective circulation through basement rock has been invoked to explain characteristics of similar strata-bound lead-zinc deposits in Ireland (Russell, 1978; Everett et al., 1999; Wilkinson et al., 2005), where field relationships show a close association with faults that penetrate metamorphic basement. Fluid inclusion data from Ireland indicate mean temperatures of ~200°C (Hitzman and Beatty, 1996), and lead isotope data suggest that the lead was derived from relatively local basement rock (LeHuray et al., 1987). Though some workers have proposed that the convective circulation in Ireland occurred in conjunction with topography-driven flow initiated during the late Paleozoic Hercynian orogeny (Hitzman and Beatty, 1996; Garven et al., 1999), the convection is now thought to have developed in an earlier, Mississippian passive margin or rift environment (Blakeman et al., 2002; Wilkinson et al., 2005).
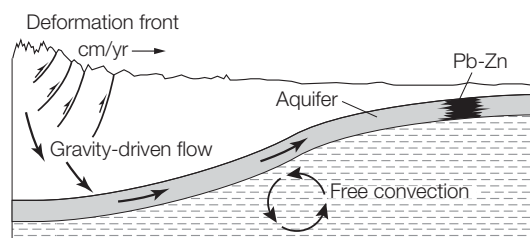


FIG. 6. Conceptual model for MVT genesis in the United States midcontinent that combines gravity-driven flow in the sedimentary section, episodic convection due to deformation-induced permeability enhancement in the underlying crystalline basement, and lead-zinc deposition at a geochemical barrier. From Deming (1992).

A more recent hypothesis for genesis of the United States MVT deposits involves gas pulsars (Cathles and Adams, 2005; Cathles, 2007). However, this hypothesis too has yet to be tested quantitatively by THMC modeling, again perhaps at least in part because of the computational challenges. This model calls for rapid, episodic brine expulsion by overpressured gas and would allow high salinity in the basin to be maintained over much longer periods of time, while still allowing for elevated heat transport and temperature at the sites of deposit formation during brief episodes of rapid flow. Huge volumes of methane-saturated low-permeability sediments ($\geq$10⁻¹⁶ m²; Cathles and Adams, 2005) are present in the central parts of many source basins (e.g., Appalachian and Arkoma basins, western Canada sedimentary basin).

*Tabular uranium deposits*

Like the MVT lead-zinc deposits of the central United States, tabular uranium deposits can be placed in the context of regional groundwater flow systems that may have extended laterally for 100s of km (Fig. 7). The important deposits of the Colorado Plateau, which account for about 65% of United States production and reserves (Chenoweth and McLemore, 1989), can be understood in the context of groundwater flow from the Mogollon Highlands (northwest Arizona) and Elko Highlands (southeast Utah) toward low-lying areas that extend north from the Four Corners region at the Utah-Colorado-Arizona-New Mexico border (Sanford, 1990, 1992, 1994; Hansley and Spirakis, 1992). This regional groundwater system reached depths of a kilometer or more, becoming highly saline as it interacted with widespread evaporites. The groundwater likely also became alkaline and possibly enriched in uranium as it altered rhyolitic ash contained in tuffaceous sandstones of the Morrison aquifer ($k \sim 10^{-13}$ m²; Thomas, 1989) to montmorillinite (Zielinski, 1982). The groundwater eventually discharged along broad paleotopographic lows where it interacted with locally derived, shallow, dilute groundwater. Some of this shallow groundwater may have originated as recharge in wetlands from which humate was transported and deposited along an interface between the dilute and saline groundwater. The humate would have served as a reductant for uranium, causing its precipitation (e.g., Langmuir, 1978; Krauskopf, 1979). A genetic relationship between tabular uranium deposits and organic reducing agents is clearly demonstrated by their intimate association with dark, pore-filling, amorphous organic material that is soluble (humate; Turner-Peterson and Hodges, 1986), and by the concentration of uranium minerals around buried logs, bone fragments, and lenses of dark shale. Codeposition of humate and uranium at a stable interface between two density-stratified fluids can explain both the tabular shape of the deposits (up to 1,000s of m in breadth by a few meters thick) and their tendency to dip away from inferred areas of groundwater discharge (Ortiz et al., 1980). Quantitative groundwater modeling has helped to constrain the driving mechanisms for fluid flow (Sanford, 1994). The flow hypothesized to have been caused by compaction of Mesozoic shale or more recent lacustrine muds would have been overwhelmed by the flow caused by the northeast-trending topographic gradient from the Mogollon highlands and, locally, by density-driven convection beneath playas.
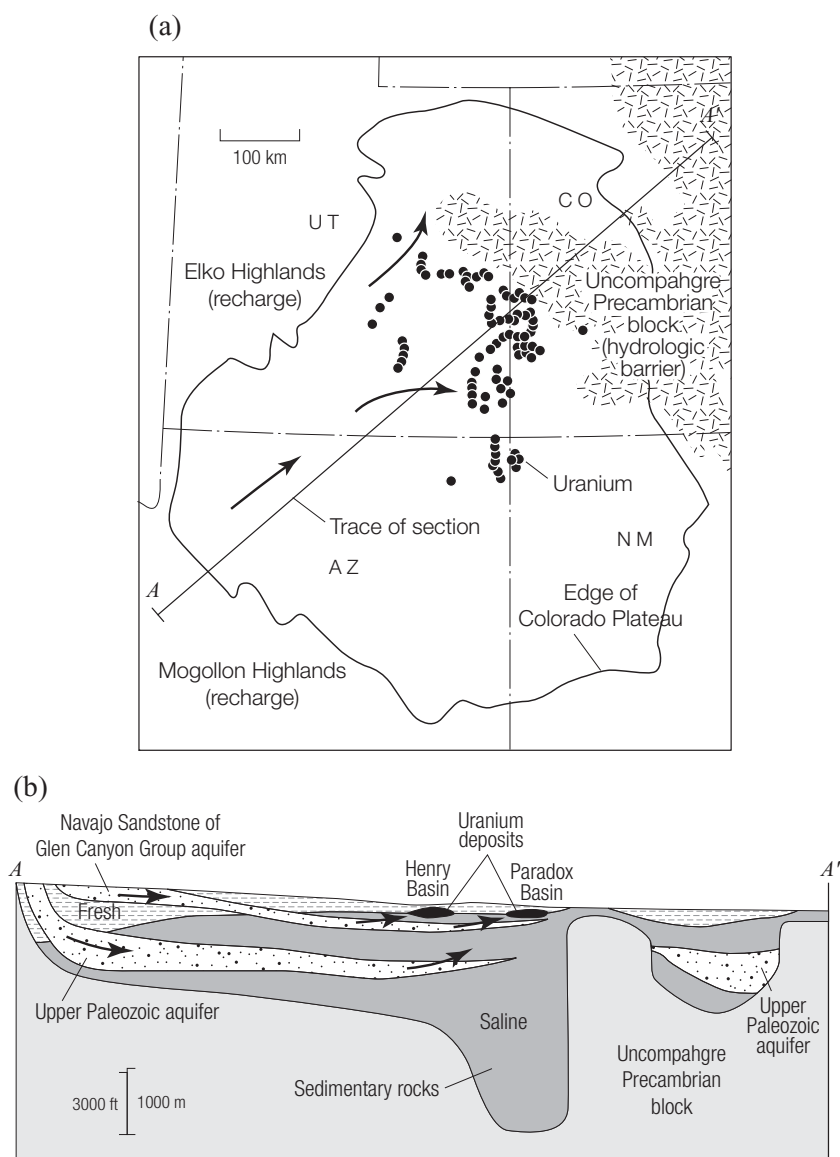
(a)



(b)



FIG. 7. (a). Map of the Colorado Plateau area showing inferred groundwater recharge areas, general direction of ground-water flow (arrows), and location of uranium deposits. (b). Southwest–northeast cross section across the Colorado Plateau, showing general direction of groundwater flow and location of uranium deposits relative to inferred position of the freshwa-ter-brine interface. In (b) the Morrison Formation overlies the Navajo Sandstone. Hydrogeologic conditions are recon-structed for the Late Jurassic (163–144 Ma). After Sanford (1992).

*Overpressured fluids in stratiform copper deposits*

Neither the MVT deposits of the United States nor the Col-orado Plateau uranium deposits show much evidence of sub-stantially elevated fluid pressures (Sanford, 1990, 1992; Pelch, 2011; Wenz et al., 2012). However, stratiform copper deposits at White Pine, Michigan, Kupferschiefer Cu-Pb-Zn deposits in Germany and Poland, and Zairian and Zambian copper deposits are attributed to compaction-driven brine upflow from permeable clastic sediments into organic- and pyrite-rich shales (Cathles and Adams, 2005). Concordant subvertical and subhorizontal veinlets and sand flames (for in-stance at White Pine) document near-lithostatic pore-fluid pressures. Modeling of elevated pore-fluid pressures as a hy-drodynamic phenomenon (generally solving eqs 1 and 4 only)

indicates that the permeability over which an active sedimen-tary basin becomes overpressured ranges from $k$ ~$10^{-20}$ to ~$10^{-17}$ m², depending on the compaction rate and the degree of overpressure (Bredehoeft and Hanshaw, 1968; Bethke, 1986; Neuzil, 1995).

*Supergene enrichment of porphyry copper deposits*

In this section we have focused on mineral deposits related to large-scale regional groundwater flow. There are also important examples of economic mineralization caused by essentially in situ diagenetic processes. Supergene enrich-ment of porphyry copper deposits has been explored with hydraulic-chemical (HC) modeling, that is, models that solve equations analogous to equations (1), (4), and (10) only.

Although porphyry copper deposits form at depth in magmatic hydrothermal systems (see "Magmatic-Hydrothermal Ore Deposits," below), many are economically viable only because they have later undergone supergene enrichment due to weathering and groundwater percolation near the water table. Pyrite and chalcopyrite weather to form hematite above the water table and chalcocite ($Cu_2S$) at and below the water table, producing an acid drainage (Sillitoe, 2005). As many of the secondary minerals are copper sulfides, mobilization of sulfur plays an important role. Early HC modeling showed that the amount of oxygen present is a key control on the system and that the dominant source of sulfur for precipitation of ore minerals was the primary minerals in the protore zone, rather than sulfate migrating from the leached zone (Ague and Brimhall, 1989). Furthermore, two end-member hydrogeologic environments of enrichment have been recognized: (1) a deep water-table environment where rapid oxidation causes a sizable oxidation blanket to develop rather quickly (in 10s of 1,000s of yrs), and (2) a shallow water-table environment with slow oxidation and enrichment that may take place over hundreds of thousands to a million years (Lichtner and Biino, 1992). The deposits in northern Chile (Alpers and Brimhall, 1988, 1989) may be an example of the former, whereas the deposits in Papua New Guinea may be an example of the latter (Bamford, 1972; Titley, 1978; Ague and Brimhall, 1989).

## Magmatic-Hydrothermal Ore Deposits

*"Much of what is known about the complex physical and chemical evolution of magmatic-hydrothermal fluids between the deep plutonic regime of granitoid intrusions and the fumarolic emanations observed in active volcanoes comes from the study of fluid inclusions in veins from … ore deposits…"* (Redmond et al., 2004)

### Characteristics of porphyry and epithermal ore deposition

Many ore deposits involving silver and gold and the sulfides of copper, molybdenum, tin, lead, zinc, and mercury are associated with magmatic heat sources and localized in vein networks that once hosted hydrothermal fluid circulation. Conceptual (Fig. 8) and semiquantitative (Fig. 9) models of fluid circulation around shallow magma bodies incorporate many important ore-forming environments. Porphyry copper deposits form in near-magma environments where reactive magmatic fluids encounter large gradients in both temperature and chemical composition (Sillitoe and Meinert, 2010). Upward movement of magmatic volatiles, involving progressive equilibration with the host rock (e.g., Reed and Palandri, 2010), can produce hydrothermal alteration in the epithermal environment characterized by low $f_{S_2}$, minerals such as adularia ($K[AlSi_3O_8]$) and sericite (fine-grained $KAl_2(OH)_2$ $[(AlSi_3)O_{10}]$), and both base and precious metal deposits. Condensation of magmatic vapors containing acidic components (HCl, $SO_2$, $H_2SO_4$) in groundwater at shallow depths under nonequilibrium conditions produces advanced argillic alteration, with minerals such as alunite ($K[Al_3(OH)_6(SO_4)_2]$) and kaolinite ($Al_4(OH)_8[Si_4O_{10}]$) plus a siliceous residue; in some cases copper and gold mineralization can form ore deposits in these environments. Porphyry ore deposits are associated with fluids of widely varying salinities, from only a few to
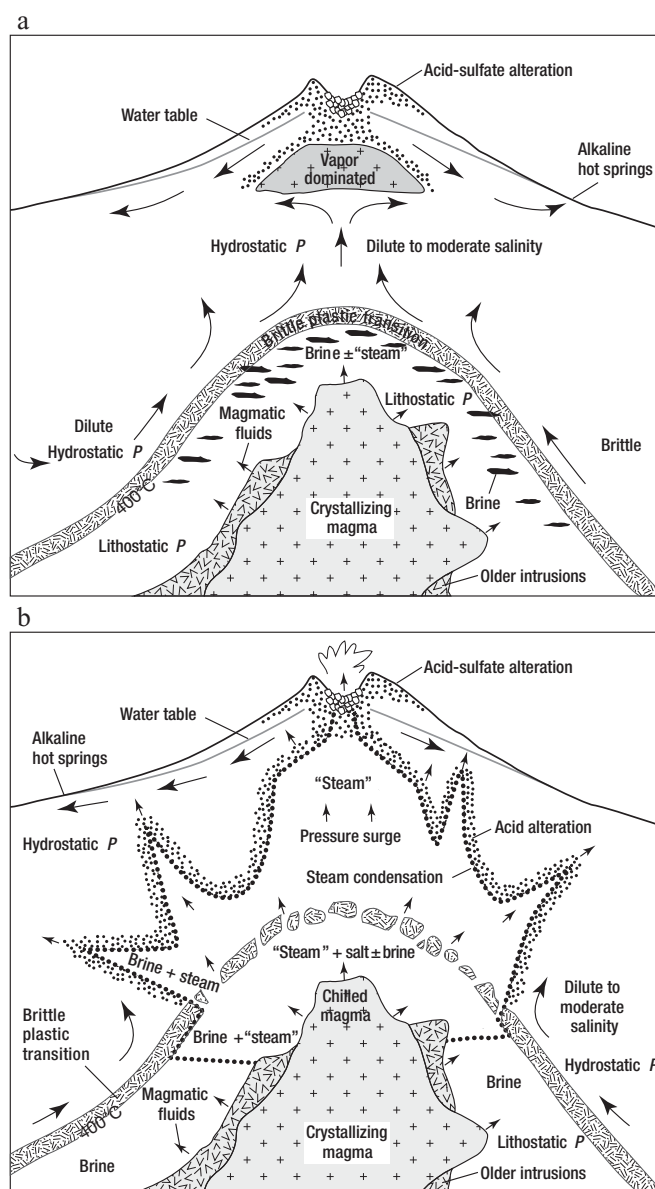


FIG. 8. Schematic diagram of a magmatic-hydrothermal system with episodic injection of magmatic fluids into a hydrothermal system otherwise dominated by meteoric water. (a). Dominantly meteoric water circulates at near-hydrostatic pressures in brittle rock while saline, dominantly magmatic fluid accumulates at near-lithostatic pressures in underlying plastic rock (T ≥370°–400°C). (b). Episodic and temporary breaching of a sealed zone allows discharge of magmatic fluids. From Fournier (1999). At depth, Fournier's "steam" may be 600° to 900°C $H_2O$ vapor with typically ~10 wt % $SO_2$, $CO_2$, $H_2S$, HCl, $N_2$, etc., whereas the "steam" on the margin of the system, at a temperature of ~100°C, has only $CO_2$ and $H_2S$ plus $N_2$; this lower temperature vapor forms the steam-heated blankets above the water table.

nearly 80 wt % NaCl equiv (Burnham, 1997; Misra, 2000; Heinrich et al., 2005). By contrast, epithermal deposits are associated with lower salinities, ranging from a high of about 23 to as low as <1 wt % NaCl equiv (Simmons et al., 2005). Many epithermal gold deposits form by boiling and loss of vapor, including $H_2S$, from a variable mixture of magmatic and meteoric fluids within 1 km of the surface (Figs. 8, 10; Simmons et al., 2005). Boiling also has the effect of raising the pH of the
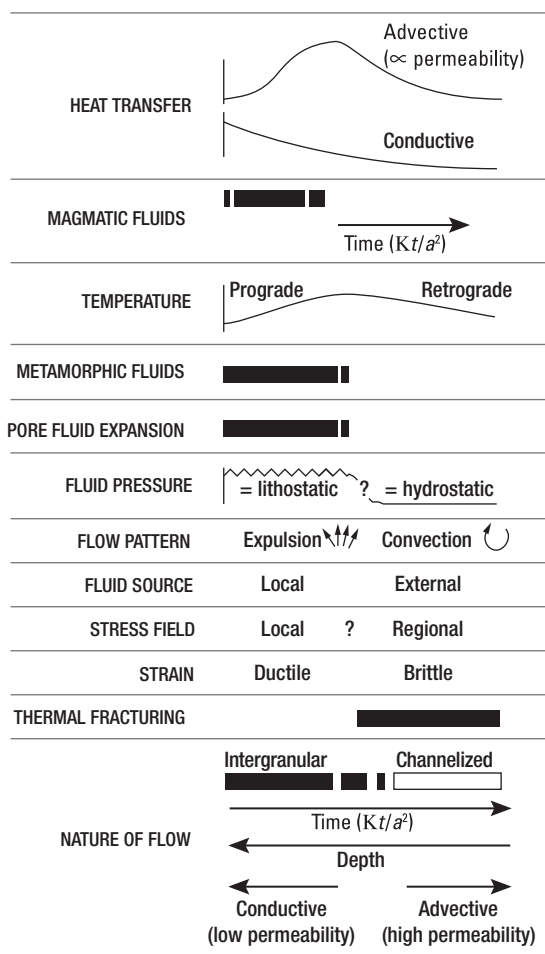
FIG. 9. Synthesis of the dynamics of heat flow, fluid flow, and deformation caused by pluton intrusion and cooling. Time variation in thermal energy that drives metamorphism and fluid movement scales with intrusion size $a$. Conductive heat flow decreases continuously with time. Fluid flow is assumed to be driven by variations in fluid density so that advective heat flow, typically most important in the host rocks, first increases as host rocks are heated by conduction across crystallizing magma, then wanes as available energy is consumed. Metamorphic fluid production and pore-fluid expansion operate only on the prograde path and are most important when the rate of heating is greatest. Together, and given sufficiently low host-rock permeability, these processes can act to maintain near-lithostatic fluid pressures and create a pervasive pore network, an expulsive pattern of fluid flow and, along with elevated temperatures, allow for ductile deformation. After peak temperatures are reached, fluid pressures tend to drop, thermal fracturing ensues, and convection-dominated flow with deeper circulation of meteoric (external) water occurs. The relative importance of advective heat-flow scales with permeability (Fig. 1, eq 4). Features on the left-hand side of the diagram are favored with increasing depth and decreasing permeability. From Hanson (1995).
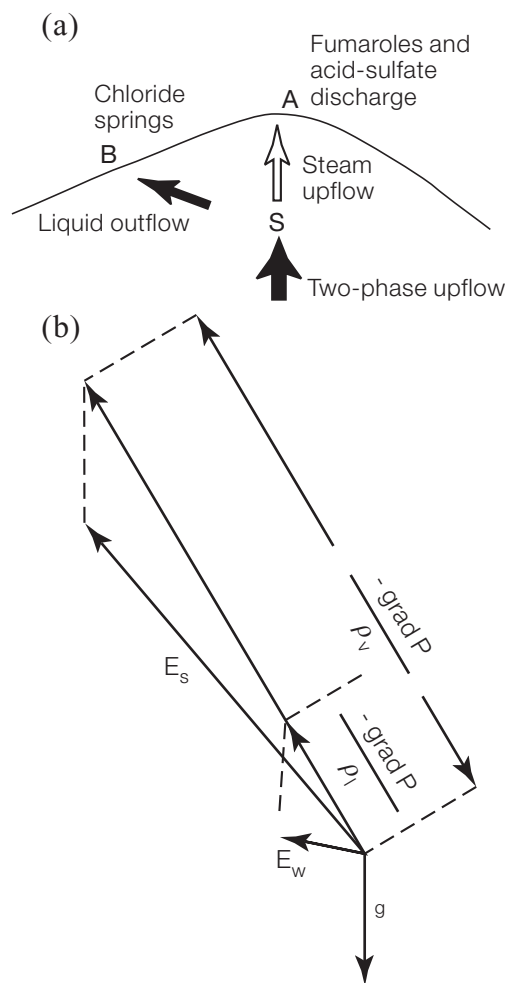


FIG. 10. (a). Schematic diagram of a high-temperature hydrothermal system at shallow depth in which boiling and phase separation takes place. (b). Impelling forces (E) acting on elements of vapor and liquid water in the area of phase separation (S) (Hubbert, 1953). Boiling-related mineralization can be concentrated near (S) in (a), where buoyant vapor separates from liquid, the former ascending and the latter flowing laterally due to the hydraulic gradient. Many epithermal gold deposits are formed by boiling (Simmons et al., 2005), which has the effect of decreasing the $H_2S$ concentration in the residual liquid because of the preferential partitioning of $H_2S$ and other volatiles to the vapor phase; this causes destabilization of the gold hydrosulfide aqueous complexes dominant in the liquid phase, yielding gold precipitation (Pokrovski et al., 2009, and references therein). After Ingebritsen and Sorey (1985).

liquid phase due to $CO_2$ loss, which can cause precipitation of calcite and/or adularia. Mixing can occur along the laterally flowing limbs of gravity- or density-driven hydrothermal systems (e.g., at Creede, Colorado; Plumlee, 1989; Hayba, 1993, 1997).

In most cases, the sources of the fluids and solutes that formed a hydrothermal ore deposit are incompletely known. Oxygen and hydrogen isotope data indicate that meteoric waters were present in many magmatic-hydrothermal environments, particularly at late stages. Oxygen isotope exchange between meteoric waters and igneous rocks results in rocks with low $^{18}O$ contents, and such $^{18}O$-depleted rocks are ubiquitous in areas of hydrothermal alteration (see e.g., the overviews by Taylor, 1979; Criss et al., 1991). There is also abundant chemical and isotopic evidence for contribution of magmatic fluids and solutes to ore-forming hydrothermal systems (e.g., Hedenquist, 1992; Hedenquist and Lowenstern, 1994). In initially low-permeability host rocks, a magmatic component dominates an early advective or expulsive stage of fluid flow (Shinohara and Hedenquist, 1997; Hedenquist et al., 1998), with the magmatic signature subsequently overprinted by that of meteoric fluids as the magmatic intrusion

finally crystallizes but remains a heat source driving convection (cf. Fig. 9).

Most hydrothermal metal deposition can be explained in terms of extreme pressure and temperature gradients, mixing, water-rock reaction, and boiling (both phase separation at a solvus at high temperature and pressure, and intersection of the saturated water-vapor curve, the latter typically at hydrostatic pressures within 1–2 km of the surface)—all phenomena that are common in magmatic-hydrothermal environments. The conceptual model of magmatic-volatile injection depicted in Figure 8 is essentially catastrophic and is in accord with a wide range of field and laboratory observations. Hydrothermal veining and brecciation commonly indicate episodic mineralization (e.g., Sibson et al., 1975) and in some instances indicate fluid pressures varying between lithostatic and hydrostatic (e.g., Gustafson and Hunt, 1975; Parry et al., 1991; Redmond et al., 2004) and extraordinary flow rates (e.g., Cathles and Shannon, 2007).

*Modeling continental magmatic-hydrothermal systems*

Complete and rigorous system-scale THMC modeling of magmatic-volatile injection is not yet possible. The state-of-the-art equations presented in the "Processes Driving Fluid Flow and Transport" section cannot fully represent the extreme pressure and temperature ranges, rapid mechanical deformation and associated permeability changes, complex water-rock interaction, and multiphase, multicomponent fluid flow ($H_2O$-$CO_2$-NaCl + other components). We must focus on a narrower subset of behaviors in order to define problems that are of interest yet quantitatively tractable.

For instance, simple reactive-solute-transport models (HC models, solving eqs 1, 4, and 10 only) of hydrothermal vein formation at the Butte, Montana, copper-porphyry system are key evidence for brief flow durations and, by inference, extraordinary flow rates. Modeling of diffusion and reaction in the Butte vein system has shown that centimeter-scale sericitic vein alteration envelopes likely require only tens of years to form by diffusive addition of $K^+$ and $H^+$ from magmatic fluids flowing through the veins (Geiger et al., 2002). Mass transport was advection dominated within veins (first term on right side of eq 10) and diffusive between veins and host rock (represented in the second term on the right side of eq 10). About 4.5 km$^3$ of the Butte Quartz Monzonite pluton were altered by ~100 km$^3$ of magmatic fluid in perhaps only a few hundred years, implying extraordinary flow rates that may have reached tens of metric tons of fluid per meter width per year in individual fractures (Cathles and Shannon, 2007), and also implying high rates of vapor emission from underlying magma (cf. Lowenstern and Hurwitz, 2008). Such flow rates are consistent with various lines of field evidence. For instance, pebble dikes are common in and near porphyry copper deposits (e.g., Gustafson and Hunt, 1975) and imply flow rates sufficient to entrain, upwardly transport, and abrade rock fragments.

Given the apparent brevity and intensity of some vein-forming episodes, it seems reasonable to equate them with what a hypothetical observer might term volcanic unrest. Episodes of rapid vein formation presumably would have entailed seismicity related to vein opening, discernible ground deformation, and obvious increases in hydrothermal venting.

High rates of vapor (and in places, metal) release have been documented at various restless volcanoes (e.g., Hedenquist et al., 1993; Goff et al., 1994), and the 1991 eruption of Pinatubo volcano in the Philippines is believed to have destroyed at least part of an incipient porphyry deposit (Hattori, 1996).

At Butte, the initial host-rock permeability at 4 to 9 km depth (Rusk et al., 2004, 2008) was insufficient to accommodate the release of the magmatic volatiles (i.e., $k \leq 10^{-17}$ m$^2$), and the near-lithostatically pressured volatiles created permeability by hydraulic fracturing, producing closely spaced (~5 cm) veinlets (Cathles and Shannon, 2007). At Bingham Canyon, Utah, another porphyry copper deposit, early quartz veins contain abundant hypersaline liquid (38–50 wt % NaCl) and vapor-rich inclusions trapped together at temperatures of 560° to 350°C and pressures of 55 to 14 MPa, consistent with fluctuations between lithostatic and hydrostatic pressure at paleodepths of 1.4 to 2.1 km (Redmond et al., 2004). During this stage, the permeability at Bingham Canyon might perhaps be conceptualized as cycling between the mean crust (blue curves) and disturbed crust (black curves) conditions of Figure 3. Cathles and Shannon (2007) suggested that early-stage quartz veins with selvages of potassic alteration may record "controlled explosions" caused by rapid exsolution of magmatic volatiles, and that the permeability created by such explosions clears the way for later ore deposition.

Given the difficulty of rigorous THMC simulation in a magmatic-hydrothermal environment, how useful are large-scale (system-wide) simulations? Strategic modeling of a subset of the actual couplings has elucidated key aspects of large-scale system behavior. For instance, thermal-hydrologic (TH) models—solving equations analogous to equations (1), (4), and (7) only—have been used to simulate the convective fluid-flow geometries associated with ore deposits in both magmatic (e.g., Eldursi et al., 2009) and nonmagmatic environments (e.g., Matthai et al., 2004; Harcoeut-Menou et al., 2009). Simulation of transient hydrothermal circulation based on typical real-world systems shows that, in general, favorable conditions for mineral deposition around midcrustal plutons develop over a short time span bracketing the hottest phase of intrusion (Eldursi et al., 2009). A model-based Rock Alteration Index analysis (the scalar product of the fluid-velocity vector and the temperature gradient) can represent the potential for mineralization (Zhao et al., 1998), assuming that advection of reactants controls the rate of mineralization and that mineral solubility decreases with decreasing temperature. Results suggest that pluton apexes (e.g., stocks) can strongly focus mineralization; that fractured, high-permeability thermal aureoles can restrict mineralization to a narrow zone bordering a stock (e.g., Scheelite Dome, Yukon); and that overlying low-angle fault-related permeability can dissipate potential mineralization from near the pluton, prevent secondary convection, and focus mineralization near the land surface (e.g., Crocetta deposit, Italy; Eldursi et al., 2009). The models employed in those studies have significant limitations, such as the inability to simulate liquid-vapor phase separation, which is likely important where intrusions are emplaced into relatively permeable crust and exsolve a magmatic fluid. Nonetheless, they seem to provide useful heuristic insights.

*Modeling mid-ocean ridge systems*

Thermal-hydrologic modeling (solution of eqs 1, 4, 7 only) has also elucidated "self-organizing" mid-ocean ridge (MOR) convection at ~400°C, where pipelike flow cells are formed due to the optimization of heat transport by water near this temperature. Volcanic massive sulfides—a type of metal-sulfide ore deposit, mainly Cu-Zn-Pb—are among the ore deposits that form in a MOR environment. A key MOR field observation is that hydrothermal-discharge temperatures appear to be limited to ~400°C, much less than the temperature of the basaltic magma that drives MOR convection. Several explanations for the limit of MOR hydrothermal temperature at ~400°C are possible. Analytical solutions for conductive heat transport (third term on the right side of eq 7) show that temperatures at the surface of a single, instantaneous intrusion will not exceed $0.5T_{max}$ (e.g., Lachenbruch et al., 1976), or ~600°C in the case of basalt. Further, for typical MOR pressures of ~40 MPa (400 bars), a maximum in silica solubility exists at ~370°C, such that circulation of higher temperature fluids may be inhibited by deposition of silica (Fournier and Potter, 1982). Finally, it has been suggested that vent temperatures are linked to the temperature of the brittle-ductile transition (Lister, 1974; Fournier, 1991).

Each of these explanations for MOR vent temperatures seems plausible, but none of them is required. Instead, numerical simulations of free convection above an arbitrarily hot base using the HYDROTHERM code (Table 3) show that the temperatures of upwelling plumes are effectively buffered by the properties of water itself. Pure water will tend to rise from an arbitrarily hot boundary layer at temperatures of 350° to 400°C, the temperature range associated with convection cells operating at maximum energy transport. This result can be understood in terms of a quantity termed "fluxibility" $F$ (Jupp and Schultz, 2000), which measures the ability of buoyancy-driven water to transport heat:

$$F = (\rho_0 - \rho)\rho H/\mu, \tag{18}$$

where $\rho_0$ is the density of cold water. For pure water, this locally defined quantity is weakly pressure dependent and shows clear peaks in $\partial F/\partial T$ at temperatures ranging from 384°C at 25 MPa to 412°C at 35 MPa. These are thus the temperatures at which pure water will tend to rise at a given pressure. The fluxibility peaks shift to somewhat higher temperatures in a seawater system. The concept of fluxibility can be extended to include both upflow (subscript $u$) and downflow (subscript $d$) zones of a hydrothermal convection cell (Coumou et al., 2008),

$$F = \frac{\rho_u (H_u - H_d)(\rho_d - \rho_u)}{\mu_u (1 + \gamma B)}, \tag{19}$$

where $\gamma$ represents the ratio $A_u k_u/A_d k_d$, $A_u$ and $A_d$ are the horizontal cross-sectional areas of the up- and downflow zones, respectively, and $B$ is the ratio of the fluid properties $\mu_d\rho_u/\mu_u\rho_d$. This version of $F$ expresses the ability of a multi-dimensional, single-phase system to transport energy by buoyancy driven convection. When evaluated, it indicates that, in a uniform-permeability medium, optimum energy transport occurs when convection cells self-organize into pipelike upflow zones (~380°C) that are surrounded by narrow zones

of focused, hot recharge (100°–300°C; see also Driesner, 2010). Numerical simulations of this process using the CSMP++ code (Table 3) indicate that recharge in MOR systems may be much more focused than had been previously assumed. Although the system depicted in Figure 11 has uniform permeability, fluid flow in both the up- and downflow zones is enhanced relative to surrounding regions by the presence of hot fluids with lower viscosity $\mu$ (see eq 1). Once established, this geometry tends to be maintained. The contrast in flow velocities caused by differences in fluid viscosity has the same stabilizing effect as a contrast in intrinsic permeability. The hot, areally restricted flow geometry dictated by water properties implies short fluid residence times.

Thus, thermal-hydrologic modeling has clearly demonstrated that both the maximum temperature and the geometry of MOR hydrothermal circulation may be greatly influenced by the properties of water itself. This is a profound result, with important implications for both proposed MOR tracer tests and the formation of massive sulfide ore deposits (Coumou et al., 2008, 2009). The self-organizing effect is not evident in a linearized "Boussinesq" fluid, for which the upflow temperature scales linearly with the basal temperature (Jupp and Schultz, 2004); its recognition required numerical models that accurately incorporate real fluid properties.

## Concluding Remarks

Hydrothermal ore deposits are the products of complex couplings between fluid flow, heat transport, solute transport,
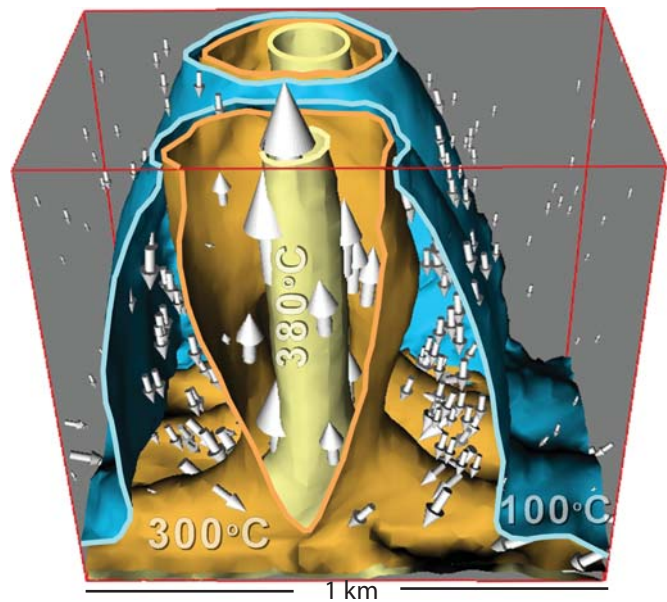


FIG. 11. Thermal and fluid-flow structure of one of nine plumes along a 4 km segment of mid-ocean ridge (MOR) axis after a simulation time of 100 years. The plume cross section shows 100°C (blue), 300°C (brown), and 380°C (yellow) isotherms as well as mass fluxes (arrows). This figure represents a 1 × 1 × 1 km portion of a 4 × 3 × 1 km model domain with a uniform permeability of $k$ = 5 × 10$^{-14}$ m$^2$ and closed lateral boundaries. The upper boundary is maintained at a constant pressure of 25 MPa with a mixed thermal boundary condition (Jupp and Schultz, 2000). A spatially variable (Gaussian) heat flux is imposed along the lower boundary, representing estimated MOR heat input of 350 MW/km of ridge length. After Coumou et al. (2008).

chemical reaction, and mechanical deformation. Quantitative models have provided valuable insights into the relevant hydrothermal processes, one of the most important of which is the fundamental role of permeability. High permeability promotes high fluid-flow rates that lead to the large heat and solute fluxes conducive to formation of ore deposits. Where permeability is low, heat and solute transport occur mainly by the relatively slow processes of conduction and diffusion. Low permeabilities, however, help make possible elevated fluid pressures due to processes such as sediment compaction, tectonic compression, fluid generation, or heating. In low-permeability rocks, fluid pressures can eventually become high enough to create new fractures, induce slip on existing faults, or trigger porosity waves to produce temporary high-permeability conduits that episodically transmit fluid, heat, and solutes. Both distribution and magnitude of permeability are important. Ore zones typically require (episodically) high permeability surrounded or capped by low-permeability zones that maintain and focus the system. Low-permeability surroundings can limit the overall permeability, allowing high temperatures to occur relatively near the surface, and stabilize the ore-forming environment, so that ore-forming processes such as boiling or mixing do not migrate widely—thus, the depth of boiling, for instance, will not change drastically as the hydrothermal system waxes and wanes. Low-permeability barriers can also allow hydrothermal systems to overpressure, fail, and depressurize, leading to boiling, and then reseal.

Transport and deformation theory have made important contributions to the understanding of ore deposits in sedimentary settings. Among the most studied are MVT deposits in the United States, where much of the focus has been on evaluating driving mechanisms for the flow of mineralizing fluids. Compaction due to sedimentation or tectonic compression has been widely discounted as an important driving mechanism for MVT ore-forming fluids, as the resulting rates of heat advection are too low to raise temperatures above conductive levels, insufficient for MVT ore formation at the expected formation depths of 1 to 1.5 km. Topographic gradients created during the orogenesis with which MVT deposits are commonly associated produce a much stronger driving force for fluid flow and, provided that permeabilities in the recharge area and ore zones were sufficiently high, topography-driven flow could have elevated ore zone temperatures to the required levels. More complex models of MVT formation have yet to be tested by quantitative coupled-process modeling.

Although topography-driven fluid flow occurs in any uplifted, subaerial terrane, it may be temporarily overwhelmed, significantly supplemented, or overprinted by other flow-driving mechanisms. Examples include the episodic flow caused by seismicity or hydrocarbon generation and the convective flow caused by a magmatic heat source. The flow regimes around magma bodies create many important classes of ore deposits, including epithermal, porphyry, and volcanogenic massive sulfide deposits. Applications of transport and deformation theory have helped to clarify the geometries of these flow regimes, the roles of magmatic and meteoric water, the locations within the flow regime where, based on maximal fluid fluxes and temperature gradients, mineralization should be concentrated, and the pressure evolution of the flow regime, which has implications for hydraulic fracturing and the formation of veins that can host mineralization. Studies of mid-ocean ridge magmatic-hydrothermal systems have shown that the transport properties of water itself may cause hydrothermal systems to self-organize into pipelike, buoyancy-driven upflow zones that are surrounded by narrow zones of focused, hot recharge.

The permeability of many ore zones is fracture dominated. Data from various modern hydrogeologic studies (e.g., Barton et al., 1995; Townend and Zoback, 2000) demonstrate that most hydraulically conductive fractures are critically stressed under the existing state of stress, whereas most fractures that are not critically stressed are nonconductive. Thus, fracture orientation relative to the (paleo) stress field may ultimately be among the most important determinants of fluid flow, transport, and ore-hosting potential.

Although much of the governing hydrogeologic theory is long established, rigorous quantification of complex process-couplings in models that incorporate site-specific geologic detail continues to be computationally challenging and represents a major research frontier. The issue of inelastic deformation and associated dynamic variations in permeability, for which fully satisfactory theory has yet to be developed, is a particular challenge. Fortunately, this problem is now under attack from several directions, as it is a core issue for emerging technologies such as Enhanced Geothermal Systems (EGS) and geologic carbon sequestration, as well as economic geology.

## Acknowledgments

## REFERENCES

Adams, J. J., and Bachu, S., 2002, Equations of state for basin geofluids: Algorithm review and intercomparison for brines: Geofluids, v. 2, p. 257–271.

Ague, J.J., and Brimhall, G.H., 1989, Geochemical modeling of steady-state fluid flow and chemical reaction during supergene enrichment of porphyry copper deposits: ECONOMIC GEOLOGY, v. 84, p. 506–528.

Alpers, C.N., and Brimhall, G.H, 1988, Middle Miocene climatic change in the Atacama Desert, northern Chile: Evidence from supergene mineralization at La Escondida: Geological Society of America Bulletin, v. 100, p. 1640–1656.

——1989, Paleohydrologic evolution and geochemical dynamics of cumulative supergene metal enrichment at La Escondida, Atacama desert, northern Chile: ECONOMIC GEOLOGY, v. 84, p. 229–254.

Appold, M.S., and Garven, G., 1999, The hydrology of ore formation in the Southeast Missouri district: Numerical models of topography-driven fluid flow during the Ouachita orogeny: ECONOMIC GEOLOGY, v. 94, p. 913–936.

——2000, Reactive flow models of ore formation in the Southeast Missouri district: ECONOMIC GEOLOGY, v. 95, p. 1605–1626.

Appold, M. S., and Nunn, J. A., 2002, Numerical models of petroleum migration via buoyancy-driven porosity waves in viscously deformable sediments: Geofluids, v. 2, p. 233–247.

——2005, Hydrology of the western Arkoma basin and Ozark platform during the Ouachita orogeny: Implications for Mississippi Valley-type ore formation in the Tri-State Zn-Pb district: Geofluids, v. 5, p. 308–325.

Appold, M.S., and Wenz, Z.J., 2011, Composition of ore fluid inclusions from the Viburnum Trend, Southeast Missouri district, United States: Implications for transport and precipitation mechanisms: ECONOMIC GEOLOGY, v. 106, p. 55–78.

Arnold, B.W., Bahr, J.M., and Fantucci, R., 1996, Paleohydrology of the Upper Mississippi Valley zinc-lead district: Society of Economic Geologists Special Publication 4, p. 378–389.

Bai, W., Xu, W., and Lowell, R.P., 2003, The dynamics of submarine heat pipes: Geophysical Research Letters, v. 30, doi:10.1029/2002GL016176.

Bamford, R.W., 1972, The Mount Fubilan (Ok Tedi) porphyry copper deposit, Territory of Papua and New Guinea: ECONOMIC GEOLOGY, v. 67, p. 1019–1033.

Barton, C.A., Zoback, M.D., and Moos, D., 1995, Fluid flow along potentially active faults in crystalline rock: Geology, v. 23, p. 683–686.

Bear, J., 1972, Dynamics of fluids in porous media: New York, Dover Publications, 764 p.

Beaumont, C., Quinlan, G.M., and Hamilton, J., 1987, The Alleghanian orogeny and its relationship to the evolution of the eastern interior, North America: Canadian Society of Petroleum Geologists Memoir 12, p. 425–445.

Benoit W.R., and Butler, R.W., 1983, A review of high-temperature geothermal developments in the northern Basin and Range province: Geothermal Resources Council, Special Report 13, p. 57–80.

Bethke, C.M., 1985, A numerical model of compaction-driven groundwater flow and its application to the paleohydrology of intracratonic sedimentary basins: Journal of Geophysical Research, v. 90, p. 6817–6828.

——1986, Inverse hydrologic analysis of the distribution and origin of Gulf Coast-type geopressured zones: Journal of Geophysical Research, v. 91, p. 6535–6545.

Bethke, C.M., and Marshak, S., 1990, Brine migrations across North America—the plate tectonics of groundwater: Annual Review of Earth and Planetary Sciences, v. 18, p. 287–315.

Bettinelli, P., Avouac, J.-P., Flouzat, M., Bollinger, L., Ramillien, G., Rajuare, S., and Sapkota, S., 2008, Seasonal variations of seismicity and geodetic strain in the Himalaya induced by surface hydrology: Earth and Planetary Science Letters, v. 266, p. 332–344.

Bickle, M.J., and McKenzie, D., 1987, The transport of heat and matter by fluids during metamorphism: Contributions to Mineralogy and Petrology v. 95, p. 644–665.

Bischoff, J.L., and Rosenbauer, R.J., 1988, Liquid-vapor relations in the critical region of the system NaCl-$H_2O$ from 380° to 415°C: A refined determination of the critical point and two-phase boundary of seawater: Geochimica et Cosmochimica Acta, v. 52, p. 2121–2126.

——1996, The alteration of rhyolite in $CO_2$ charged water at 200° and 350°C: The unreactivity of $CO_2$ at higher temperature: Geochimica et Cosmochimica Acta, v. 60, p. 3859–3867.

Bischoff, J.L., Rosenbauer, R.J., and Fournier, R.O., 1996, The generation of HCl in the system $CaCl_2$-$H_2O$: Vapor-liquid relations from 380°-500°C: Geochimica et Cosmochimica Acta, v. 60, p. 7–16.

Blackwell, D.D., and Steele, J.L., 1989, Thermal conductivity of sedimentary rocks: measurement and significance, in Naeser, N.D., and McCulloh, T.H., eds., Thermal history of sedimentary basins: New York, Springer Verlag, p. 13–36.

Blakeman, R.J., Ashton, J.H., Boyce, A.J., Fallick, A.E., and Russell, M.J., 2002, Timing of interplay between hydrothermal and surface fluids in the Navan Zn + Pb orebody, Ireland: Evidence from metal distribution trends, mineral textures, and $\delta^{34}S$ analyses: ECONOMIC GEOLOGY, v. 97, p. 73–91.

Bollinger, L., Perrier, F., Avouac, J.-P., Sapkota, S., Gautam, U., and Tiwari, D.R., 2007, Seasonal modulation of seismicity in the Himalaya of Nepal: Geophysical Research Letters, v. 34, doi:10.1029/2006GL029192.

Bower, K.M., and Zyvoloski, G., 1997, A numerical model for thermo-hydromechanical coupling in fractured rock: International Journal of Rock Mechanics and Mineral Science, v. 34, p. 1201–1211.

Brace, W.F., 1980, Permeability of crystalline and argillaceous rocks: International Journal of Rock Mechanics and Mining Sciences and Geomechanics Abstracts, v. 17, p. 241–251.

Brannon, J.C., Cole, S.C., Podosek, F.A., Ragan, V.M., Coveney, R.M., Jr., Wallace, M.W., and Bradley, A.J., 1996a, Th-Pb and U-Pb dating of ore-stage calcite and Paleozoic fluid flow: Science, v. 271, p. 491–493.

Brannon, J.C., Cole, S.C., and Podosek, F.A., 1996b, Radiometric dating of Mississippi Valley-type Pb-Zn deposits: Society of Economic Geologists Special Publication 4, p. 536–545.

Bredehoeft, J.D., and Hanshaw, B.B., 1968, On the maintenance of anomalous fluid pressures: I. Thick sedimentary sequences: Geological Society of America Bulletin, v. 79, p. 1097–1106.

Bredehoeft, J.D., and Papadopolous, I.S., 1965, Rates of vertical groundwater movement estimated from the Earth's thermal profile: Water Resources Research, v. 1, p. 325–328.

Burnett, R.D., and Frind, E.O., 1987, An alternative direction Galerkin technique for simulation of groundwater contamination transport in three dimensions, 2 dimensionality effects: Water Resources Research, v. 23, p. 695–705.

Burnham, W.C., 1997, Magmas and hydrothermal fluids, in Barnes, H.L., ed., Geochemistry of hydrothermal ore deposits, 3rd ed.: New York, Wiley and Sons, p. 63–123.

Cathles, L.M., III, 2007, Changes in sub-water table flow at the end of the Proterozoic and its implications for gas pulsars and MVT lead-zinc deposits: Geofluids, v. 7, p. 209–226.

Cathles, L.M., and Adams, J.J., 2005, Fluid flow and petroleum and mineral resources in the upper (<20 km) continental crust: ECONOMIC GEOLOGY 100TH ANNIVERSARY VOLUME, p. 77–110.

Cathles, L.M., and Shannon, R., 2007, How potassium silicate alteration suggests the formation of porphyry ore deposits began with the nearly explosive but barren expulsion of large volumes of magmatic water: Earth and Planetary Science Letters, v. 262, p. 92–108.

Cathles, L.M., and Smith, A.T., 1983, Thermal constraints on the formation of Mississippi Valley-type lead-zinc deposits and their implications for episodic basin dewatering and deposit genesis: ECONOMIC GEOLOGY, v. 78, p. 983–1002.

Chenoweth, W.L., and McLemore, V.T., 1989, Uranium resources on the Colorado Plateau, in Lorenz, J.C., and Lucas, S.G., eds., Energy frontier in the Rockies: Albuquerque, New Mexico, Albuquerque Geological Society, xxx p.

Christiansen, L.B., Hurwitz, S., Saar, M.O., Hsieh, P.A., and Ingebritsen, S.E., 2005, Seasonal seismicity at western United States volcanoes: Earth and Planetary Science Letters, v. 240, p. 307–321.

Christiansen, L.B., Hurwitz, S., and Ingebritsen, S.E., 2007, Annual modulation of seismicity along the San Andreas Fault near Parkfield, CA: Geophysical Research Letters, v. 34, L04306, doi:10.1029/2006GL028634.

Connolly, J.A.D., 1997, Devolatilization-generated fluid pressure and deformation-propagated fluid flow during prograde regional metamorphism: Journal of Geophysical Research, v. 102, p. 18,149–18,173.

Corey, A.T., 1954, The interrelations between gas and oil relative permeabilities: Producers Monthly, v. 19, p. 38–41.

Coumou, D., 2008, Numerical simulation of fluid flow in mid-ocean ridge hydrothermal systems: Unpublished Ph.D. thesis, Zurich, Switzerland, ETH-Zurich, 163 p.

Coumou, D., Driesner, T., and Heinrich, C.A., 2008, The structure and dynamics of mid-ocean ridge hydrothermal systems: Science, v. 321, p. 1825–1828.

Coumou, D., Weiss, P., Driesner, T., and Heinrich, C.A., 2009, Phase-separation, brine formation, and salinity variation in Black Smoker hydrothermal systems: Journal of Geophysical Research, v. 114, doi:10.1029/2008JB005764.

Coveney, R.M., Jr., Goebel, E.D., and Ragan, V.M., 1987, Pressures and temperatures from aqueous fluid inclusions in sphalerite from mid-continent country rocks: ECONOMIC GEOLOGY, v. 82, p. 740-751.

Coveney, R.M., Jr., Ragan, V.M., and Brannon, J. C., 2000, Temporal benchmarks for modeling Phanerozoic flow of basinal brines and hydrocarbons in the southern midcontinent based on radiometrically dated calcite: Geology, v. 28, p. 795–798.

Cox, S.F., 2002, Fluid flow in mid- to deep crustal shear systems: Experimental constraints, observations on exhumed high fluid flux shear systems, and implications for seismogenic processes: Earth Planets Space, v. 4, p. 1121–1125.

——2005, Coupling between deformation, fluid pressures, and fluid flow in ore-producing hydrothermal sytems at depth in the crust: ECONOMIC GEOLOGY 100TH ANNIVERSARY VOLUME, p. 39–75.

Criss, R.E., Fleck, R.J., and Taylor, H.P., Jr., 1991, Tertiary meteoric hydrothermal systems and their relation to ore deposition, northwestern United States and southern British Columbia: Journal of Geophysical Research, v. 96, p. 13,335–13,356.

Darcy, H.P.G., 1856, Les Fontaines Publiques de la Ville de Dijon: Paris, Victor Dalmont.

Domenico, P.A., and Mifflin, M.D., 1965, Water from low-permeability sediments and land subsidence: Water Resources Research, v. 1, p. 563–576.

Deming, D., 1992, Catastrophic release of heat and fluid flow in the continental crust: Geology, v. 20, p. 83–86.

Deming, D., and Nunn, J.A., 1991, Numerical simulations of brine migration by topographically driven recharge: Journal of Geophysical Research, v. 96, p. 2485–2499.

Driesner, T., 2007, The system $H_2O$-NaCl. Part II: Correlations for molar volume, enthalpy, and isobaric heat capacity from 0 to 1000°C, 1 to 5000 bar, and 0 to 1 $X_{NaCl}$: Geochimica et Cosmochimica Acta, v. 71, p. 4902–4919.

——2010, The interplay of permeability and fluid properties as a first order control of heat transport, venting temperatures and venting salinities at mid-ocean ridge hydrothermal systems: Geofluids, v. 10, p. 132–141.

Driesner, T., and Geiger, S., 2007, Numerical simulation of multiphase fluid flow in hydrothermal systems: Reviews in Mineralogy and Geochemistry, v. 65, p. 187–212.

Dutrow, D., and Norton, D., 1995, Evolution of fluid pressure and fracture propagation during contact metamorphism: Journal of Metamorphic Geology, v. 13, p. 677–686.

Dutrow, B.L., Travis, B.J., Gable, C.W., and Henry, D.J., 2001, Coupled heat and silica transport associated with dike intrusion into sedimentary rock: Effects on isotherm location and permeability evolution: Geochimica et Cosmochimica Acta, v. 65, p. 3749–3767.

Eldursi, K., Branquet, Y., Guillou-Trottier, L., and Marcoux, E., 2009, Numerical investigation of transient hydrothermal processes around intrusions: Heat-transfer and fluid-circulation controlled mineralization patterns: Earth and Planetary Science Letters, v. 288, p. 70–83.

Elkhoury, J.E., Brodsky, E.E., and Agnew, D.C., 2006, Seismic waves increase permeability: Nature, v. 441, p. 1135–1138.

Everett, C.E., Wilkinson, J.J., and Rye, D.M., 1999, Fracture-controlled fluid flow in the lower Palaeozoic basement rocks of Ireland: Implications for the genesis of Irish-type Zn-Pb deposits: Geological Society [London] Special Publication 155, p. 247–276.

Fairley, J.P., Ingebritsen, S.E., and Podgorney, R.K., 2010, Challenges for modeling of enhanced geothermal systems: Ground Water, v. 48, p. 482–483.

Faust, C.R., and Mercer, J.W., 1979, Geothermal reservoir simulation. 1. Mathematical models for liquid- and vapor-dominated hydrothermal systems: Water Resources Research, v. 15, p. 23–30.

Ferry, J.M., 1992, Regional metamorphism of the Waits River Formation, eastern Vermont: Delineation of a new type of giant metamorphic hydrothermal system: Journal of Petrology, v. 33, p. 45–94.

Fetter, C.W., 2001, Applied hydrogeology, 4th ed.: Upper Saddle River, New Jersey, Prentice Hall, 598 p.

Finlayson, B.A., 1992, Numerical methods for problems with moving fronts: Seattle, Washington, Ravenna Park Publishing.

Forster, C., and Smith, L., 1989, The influence of groundwater flow on thermal regimes in mountainous terrain: A model study: Journal of Geophysical Research, v. 97, p. 9439–9451.

Fournier, R.O., 1991, The transition from hydrostatic to greater than hydrostatic fluid pressure in presently active continental hydrothermal systems in crystalline rock: Geophysical Research Letters, v. 18, p. 955–958.

——1999, Hydrothermal processes related to movement of fluid from plastic into brittle rock in the magmatic-epithermal environment: ECONOMIC GEOLOGY, v. 94, p. 1193–1211.

Fournier, R.O., and Potter, R.W., 1982, A revised and expanded silica (quartz) geothermometer: Geothermal Resources Council Bulletin v. 11, no. 10, p. 3–9.

Foustoukos, D.I., and Seyfried, W.E., Jr., 2007, Fluid phase separation processes in submarine hydrothermal systems: Reviews in Mineralogy and Geochemistry, v. 65, p. 213–239.

Freeze, R.A., and Cherry, J.A., 1979, Groundwater: Englewood Cliffs, Prentice Hall.

Freeze, R.A., and Witherspoon, P.A., 1967, Theoretical analysis of regional groundwater flow. 2. Effect of water-table configuration and subsurface permeability variation: Water Resources Research, v. 3, p. 623–634.

Fyfe, W.S., Price, N.J., and Thompson, A.B., 1978, Fluids in the Earth's crust: New York, Elsevier Scientific.

Garven, G., 1985, The role of regional fluid flow in the genesis of the Pine Point deposit, Western Canada sedimentary basin: ECONOMIC GEOLOGY, v. 80, p. 307–324.

——1989, A hydrogeologic model for the formation of the giant oil sands deposits of the Western Canada sedimentary basin: American Journal of Science, v. 289, p. 105–166.

Garven, G., and Freeze, R.A., 1984a, Theoretical analysis of the role of groundwater flow in the genesis of stratabound ore deposits. 1. Mathematical and numerical model: American Journal of Science, v. 284, p. 1085–1124.

——1984b, Theoretical analysis of the role of groundwater flow in the genesis of stratabound ore deposits. 2. Quantitative results: American Journal of Science, v. 284, p. 1125–1174.

Garven, G., and Raffensperger, J. P., 1997, Hydrogeology and geochemistry of ore genesis in sedimentary basins, in Barnes, H. L., ed., Geochemistry of hydrothermal ore deposits, 3rd ed.: New York, Wiley and Sons, p. 125–189.

Garven, G., Ge, S., Person, M.A., and Sverjensky, D.A., 1993, Genesis of stratabound ore deposits in the midcontinent basins of North America. 1. The role of regional groundwater flow: American Journal of Science, v. 293, p. 497–568.

Garven, G., Appold, M.S., Toptygina, V.I., and Hazlett, T.J., 1999, Hydrogeologic modeling of the genesis of carbonate-hosted led-zinc ores: Hydrogeology Journal, v. 7, p. 108–126.

Gaylord, W. B., 1995, Geology of the Elmwood and Gordonsville mines, Central Tennessee zinc district—an update: Society of Economic Geologists Guidebook Series, v. 22, p. 173–204.

Ge, S., and Garven, G., 1992, Hydromechanical modeling of tectonically driven groundwater flow with application to the Arkoma foreland basin: Journal of Geophysical Reseach, v. 97, p. 9119–9144.

Geiger, S., Haggerty, R., Dilles, J.H., Reed, M.H., and Matthai, S.K., 2002, New insights from reactive solute transport modeling: The formation of sericitic vein envelopes during early hydrothermal alteration at Butte, Montana: Geofluids, v. 2, p. 185–201.

Giggenbach, W.F., 1984, Mass transfer in hydrothermal alteration systems—a conceptual approach: Geochimica et Cosmochimica Acta, v. 48, p. 2693–2711.

Gleeson, T., Smith, L., Moosdorf, N., Hartmann, J., Durr, H.H., Manning, A.H., van Beek, L.P.H., and Jellinek, A.M., 2011, Mapping permeability over the surface of the Earth: Geophysical Research Letters, v. 38, doi:10.1029/2010GL045565.

Goff, F., Stimac, J.A., Laroque, A.C.L., Hulen, J.B., McMurtry, G.M., Adams, A.I., Roldan-M., A., Trujillo, P.E., Jr., Counce, D., Chipera, S.J., Mann, D., and Heizler, M., 1994, Gold degassing and deposition at Galeras volcano, Colombia: GSA Today, v. 4, p. 241, 244–247.

Goldhaber, M.G., Church, S.E., Doe, B.R., Aleinikoff, J.M., Brannon, J.C., Podosek, F.A., Mosier, E.L., Taylor, C.D., and Gent, C.A., 1995, Lead- and sulfur-isotope investigations of Paleozoic sedimentary rocks from the southern mid-continent of the United States: Implications for paleohydrology and ore genesis of the Southeast Missouri lead belts: ECONOMIC GEOLOGY, v. 90, p. 1875–1910.

Grogan, R.M., and Bradbury, J.C., 1968, Fluorite-zinc-lead deposits of the Illinois Kentucky mining district, in Ridge, J.D., ed., Ore deposits of the United States, 1933–1967 (Graton Sales volume): New York, American Institute of Mining, Metallurgical, and Petroleum Engineers, p. 370–399.

Gruen, G., Heinrich, C.A., Schroeder, K., and Meinert, L.D., 2010, The Bingham Canyon porphyry Cu-Mo-Au deposit, II: Vein geometry and ore shell formation by pressure-driven rock extension: ECONOMIC GEOLOGY, v. 105, p. 69–90.

Gustafson, L.B., and Hunt, J.P., 1975, The porphyry copper deposit at El Salvadore, Chile: ECONOMIC GEOLOGY, v. 70, p. 857–912.

Haar, L., Gallagher, J.S., and Kell, G.S., 1984, NBS/NRC steam tables: Thermodynamic and transport properties and computer programs for vapor and liquid states of water in SI units: New York, Hemisphere Publishing.

Hainzl, S., Kraft, T., Wassenman, J., Igel, H., and Schmedes, E., 2006, Evidence for rainfall-triggered earthquake activity: Geophysical Research Letters, v. 33, doi:10.1029/2006GL027642.

Haney, M.M., Sneider, R., Sheiman, J., and Losh, S., 2005, A moving fluid pulse in a fault zone: Nature, v. 437, p. 46.

Hanor, J.S., 1996, Controls on the solubilization of lead and zinc in basinal brines: Society of Economic Geologists Special Publication 4, p. 483–500.

Hansley, P.L., and Spirakis, C.S., 1992, Organic matter diagenesis as the key to a unifying theory for the genesis of tabular uranium-vanadium deposits in the Morrison Formation, Colorado Plateau: ECONOMIC GEOLOGY, v. 87, p. 352–365.

Hanson, R.B., 1992, Effects of fluid production on fluid flow during regional and contact metamorphism: Journal of Metamorphic Geology, v. 10, 87–97.

——1995, The hydrodynamics of contact metamorphism: Geological Society of America Bulletin, v. 107, p. 595–611.

——1997, Hydrodynamics of regional metamorphism due to continental collision: ECONOMIC GEOLOGY, v. 92, p. 880–891.

Harcouet-Menou, V., Guillou-Trottier, L., Bonneville, A., and Adler, P.M., 2009, Hydrothermal convection in and around mineralized fault zones: Insights from two- and three-dimensional numerical modeling applied to the Ashanti belt, Ghana: Geofluids, v. 9, p. 116–137.

Hattori, K., 1996, Occurrence and origin of sulfide and sulfate in the 1991 Mount Pinatubo eruption products, *in* Newhall, C.G., and Punongbayan, R.S., eds., Fire and mud: Eruptions and lahars of Mount Pinatubo, Philippines: Quezon City, Philippines, Philippine Institute of Volcanology and Seismology, p. 807–824.

Hayba, D. O., 1993, Numerical hydrologic modeling of the Creede epithermal ore-forming system: Unpublished Ph.D. thesis, Champaign-Urbana, Illinois, University of Illinois, 186 p.

——1997, Environment of ore deposition in the Creede mining district, San Juan Mountains, Colorado: Part V. Epithermal mineralization from fluid mixing in the OH vein: ECONOMIC GEOLOGY, v. 92, p. 29–44.

Hayba, D.O., and Ingebritsen, S.E., 1994, The computer model HYDROTHERM, a three-dimensional finite-difference model to simulate ground-water flow and heat transport in the temperature range of 0 to 1,200°C: U.S. Geological Survey Water-Resources Investigations Report 94-4045.

——1997, Multiphase groundwater flow near cooling plutons: Journal of Geophysical Research, v. 102, p. 12,235–12,252.

Hedenquist, J.W., ed., 1992, Magmatic contributions to hydrothermal systems and the behavior of volatiles in magma: Geological Survey of Japan Report 279.

Hedenquist, J.W., and Lowenstern, J.L., 1994, The role of magmas in the formation of hydrothermal ore deposits: Nature, v. 370, p. 519–527.

Hedenquist, J.W., Simmons, S.F., Giggenbach, W.F., and Eldridge, C.S., 1993, White Island, New Zealand, volcanic-hydrothermal system represents the geochemical environment for high sulfidation Cu and Au ore deposition: Geology, v. 21, p. 731–734.

Hedenquist, J.W., Arribas, A., and Reynolds, T.J., 1998, Evolution of an intrusion-centered hydrothermal system; Far Southeast-Lepanto porphyry and epithermal Cu-Au deposits, Philippines: ECONOMIC GEOLOGY, v. 93, p. 373–404.

Heinrich, C.A., Andrew, A.S., and Knil, M.D., 2000, Regional metamorphism and ore formation: Evidence from stable isotopes and other fluid: Reviews in Economic Geology, v. 11, p. 97–117.

Heinrich, C.A., Halter, W., Landtwing, M.R., and Pettke, T., 2005, The formation of economic porphyry copper (-gold) deposits: Constraints from microanalysis of fluid and melt inclusions: Geological Society [London] Special Publication 248, p. 247–263.

Heki, K., 2001, Seasonal modulation of interseismic strain buildup in northeastern Japan driven by snow loads: Science, v. 293, p. 89–92.

——2003, Snow load and seasonal variation of earthquake occurrence in Japan: Earth and Planetary Science Letters, v. 207, p. 159–164.

Henderson P., and Henderson, G.M., 2009, The Cambridge handbook of earth science data: Cambridge, United Kingdom, Cambridge University Press, 277 p.

Henley, R.W., and Hughes, G.O., 2000, Underground fumaroles: "Excess heat" effects in vein formation: ECONOMIC GEOLOGY, v. 95, p. 453–466.

Heyl, A.V., 1968, The Upper Mississippi Valley base-metal district, *in* Ridge, J.D., ed., Ore deposits of the United States, 1933–1967 (Graton-Sales volume): New York, American Institute of Mining, Metallurgical, and Petroleum Engineers, p. 431–459.

Heyl, A.V., Delevaux, M.H., Zartman, R.E., and Brock, M.R., 1966, Isotopic study of galenas from the upper Mississippi Valley, the Illinois-Kentucky, and some Appalachian valley mineral districts: ECONOMIC GEOLOGY, v. 61, p. 933–961.

Hitzman, M.W., and Beaty, D.W., 1996, The Irish Zn-Pb-(Ba) orefield: Society of Economic Geologists Special Publication 4, p. 112–143.

Hochstein, M.P., and Browne, P.R.L., 2000, Surface manifestations of geothermal systems with volcanic heat sources, *in* Sigurdsson, H., Houghton, B.F., McNutt, S.R., Rymer, H., and Stix, J., eds., Encyclopedia of volcanoes: San Diego, Academic Press, p. 835–855.

Horne, R.N., Satik, C., Mahiya, G., Li, K., Ambusso, W., Tovar, R., Wang, C., and Nassori, H., 2000, Steam-water relative permeability: Geothermal Resources Council Transactions, v. 24, p. 597–604.

Hsieh, P.A., and Bredehoeft, J.D., 1981, A reservoir analysis of the Denver earthquakes: A case of induced seismicity: Journal of Geophysical Research, v. 86, p. 903–920.

Huizenga, J., Gutzmer, J., Banks, D., and Greyling, L., 2006, The Paleoproterozoic carbonate-hosted Pering Zn-Pb deposit, South Africa. II: Fluid inclusion, fluid chemistry and stable isotope constraints: Mineralium Deposita, v. 40, p. 686–706.

Hurwitz, S., Kipp, K.L., Ingebritsen, S.E., and Reid, M.E., 2003, Groundwater flow, heat transport, and water table position within volcanic edifices: Implications for volcanic processes in the Cascade Range: Journal of Geophysical Research, v. 108, doi:10.1029/2003JB002565.

Hurwitz, S., Christiansen, L.B., and Hsieh, P.A., 2007, Hydrothermal fluid flow and deformation in large calderas: Inferences from numerical simulations: Journal of Geophysical Research, v. 112, doi:10.1029/2006JB004689.

Ingebritsen, S.E., and Manning, C.E., 1999, Geological implications of a permeability-depth curve for the continental crust: Geology, v. 27, p. 1107–1110.

——2002, Diffuse fluid flux through orogenic belts: Implications for the world ocean: Proceedings of the National Academy of Sciences, v. 99, p. 9113–9116.

——2010, Permeability of the continental crust: Dynamic variations inferred from seismicity and metamorphism: Geofluids, v. 10, p. 193–205.

Ingebritsen, S.E., and Mariner, R.H., 2010, Hydrothermal heat discharge in the Cascade Range, northwestern United States: Journal of Volcanology and Geothermal Research, v. 196, p. 208–218, doi:10.1016/j.volgeores.2010.07.023.

Ingebritsen, S.E., and Sorey, M.L., 1985, A quantitative analysis of the Lassen hydrothermal system, north-central California: Water Resources Research, v. 21, p. 853–868.

Ingebritsen, S.E., Sanford, W.E., and Neuzil, C.E., 2006, Groundwater in geologic processes, 2nd ed.: Cambridge, UK, Cambridge University Press, 451 p.

Ingebritsen, S.E., Geiger, S., Hurwitz, S., and Driesner, T., 2010, Numerical simulation of magmatic hydrothermal systems: Reviews of Geophysics, v. 48, RG1002, doi:10.1029/2009RG000287.

Jessop, A.M., 1990, Thermal geophysics: Amsterdam, Elsevier, 306 p.

Jolly, J.L., and Heyl, A.V., 1964, Mineral paragenesis and zoning in the Central Kentucky mineral district: ECONOMIC GEOLOGY, v. 59, p. 596–624.

Jowett, E.C., 1987, Formation of sulfide-calcite veinlets in the Kupferschiefer Cu-Ag deposits in Poland by natural hydrofracturing during basin subsidence: Journal of Geology, v. 95, p. 513–526.

Jupp, T., and Schultz, A., 2000, A thermodynamic explanation for black smoker temperatures: Nature, v. 403, p. 880–883.

——2004, Physical balances in subseafloor hydrothermal convection cells: Journal of Geophysical Research, v. 109, doi:10.1029/2003JB002697.

Keating, G.N., Geissman, J.W., and Zyvoloski, G.A., 2002, Multiphase modeling of contact metamorphic systems and application to transitional geomagnetic fields: Earth and Planetary Science Letters, v. 198, p. 429–448.

Kipp, K.L., Jr., Hsieh, P.A., and Charlton, S.R., 2008, Guide to the revised ground-water flow and heat transport simulator: HYDROTHERM–Version 3: U.S. Geological Survey Techniques and Methods 6-A25.

Kissling, W.M., 2005, Transport of three-phase hyper-saline brines in porous media: Examples: Transport in Porous Media, v. 60, p. 141–157.

Kohl, T., and Megel, T., 2007, Predictive modeling of reservoir response to hydraulic stimulations at the European EGS site Soultz-sous-Forets: International Journal of Rock Mechanics and Mining Sciences, v. 44, p. 1118–1131.

Krauskopf, K.B., 1979, Introduction to geochemistry: New York, New York, McGraw-Hill, 617 p.

Lachenbruch, A.H., Sass, J.H., Munroe, R.J., and Moses, T.H., Jr., 1976, Geothermal setting and simple heat-conduction models for the Long Valley caldera: Journal of Geophysical Research, v. 81, p. 769–784.

Langmuir, D., 1978, Uranium solution-mineral equilibria at low temperatures with applications to sedimentary ore deposits: Geochimica et Cosmochimica Acta, v. 42, p. 547–579.

Leach, D.L., 1994, Genesis of the Ozark Mississippi Valley-type metallogenic province, Missouri, Arkansas, Kansas, and Oklahoma, USA, *in* Fontboté, L., and Boni, M., eds., Sediment-hosted Zn-Pb ores: Berlin-Heidelberg, Springer-Verlag, p. 104–138.

Leach, D.L., and Sangster, D.F., 1993, Mississippi Valley-type lead-zinc deposits: Geological Association of Canada Special Paper 40, p. 289–314.

Leach, D.L., Bradley, D.C., Huston, D., Pisarevsky, S.A., Taylor, R.D., and Gardoll, S.J., 2010, Sediment-hosted lead-zinc deposits in Earth history: ECONOMIC GEOLOGY, v. 105, p. 593–625.

LeHuray, A.P., Caulfield, J.B.D., Rye, D.M., and Dixon, P.R., 1987, Basement controls on sediment-hosted Zn-Pb deposits: A Pb isotope study of Carboniferous mineralization in central Ireland: ECONOMIC GEOLOGY, v. 82, p. 1695–1709.

Lewis, K. C., 2007, Numerical modeling of two-phase flow in the sodium chloride-water system with applications to seafloor hydrothermal systems: Unpublished Ph.D. thesis, Atlanta, Georgia, Georgia Institute of Technology, 143 p.

Lewis, K.C., and Lowell, R.P., 2009, Numerical modeling of two-phase flow in the NaCl-H$_2$O system: Introduction of a numerical method and benchmarking: Journal of Geophysical Research, v. 114, doi:10.1029JB006029.

Lichtner, P.C., and Biino, G.G., 1992, A first principles approach to supergene enrichment of a porphyry copper protore: I. Cu-Fe-S subsystem: Geochimica et Cosmochimica Acta, v. 56, p. 3987–4013.

Liebscher, A., 2010, Aqueous fluids at elevated pressure and temperature: Geofluids, v. 10, p. 3–19.

Lister, C.R.B., 1974, On the penetration of water into hot rock: Geophysical Journal of the Royal Astronomical Society, v. 39, p. 465–509.

Lowell, R.P., and Xu, W., 2000, Sub-critical two-phase seawater convection near a dike: Earth and Planetary Science Letters, v. 174, p. 385–396.

Lowenstern, J.B., and Hurwitz, S., 2008, Monitoring a supervolcano in repose: Heat and volatile flux at the Yellowstone caldera: Elements, v. 4, p. 35–40.

Lu, X., and Kieffer, S.W., 2009, Thermodynamics and mass transport in multicomponent, multiphase H$_2$O systems of planetary interest: Annual Reviews of Earth and Planetary Science, v. 37, p. 449–477.

Lucente, F.P., De Gori, P., Margheriti, L., Piccinni, D., Di Bona, M., Chiarabba, C., and Agostinetti, N.P., 2010, Temporal variation of seismic velocity and anisotropy before the 2009 $M_w$ 6.3 L'Aquila, Italy earthquake: Geology, v. 38, p. 1015–1018.

Lyubetskaya, T., and Ague, J.J.. 2009, Modeling the magnitudes and directions of regional metamorphic fluid flow in collisional orogens: Journal of Petrology, v. 50, p. 1505–1531.

Manga, M., 1998, Advective heat transport by low-temperature discharge in the Oregon Cascades: Geology, v. 26, p. 799–802.

Manga, M., and Rowland, J.C., 2009, Response of Alum Rock springs to the October 30, 2007 Alum Rock earthquake and implications for the origin of increased discharge after earthquakes: Geofluids, v. 9, p. 237–250.

Manning, C.E., and Ingebritsen, S.E., 1999, Permeability of the continental crust: The implications of geothermal data and metamorphic systems: Reviews of Geophysics, v. 37, p. 127–150.

Matthai, S.K., Heinrich, C.A., and Driesner, T., 2004, Is the Mount Isa copper deposit the product of forced brine convection in the footwall of a major reverse fault?: Geology, v. 32, p. 357–360.

Matthäi, S.K., Geiger, S., Roberts, S.G., Paluzny, A., Belayneh, M., Burri, A., Mezentsev, A., Lu, H., Coumou, D., Driesner, T., and Heinrich, C.A., 2007, Numerical simulations of multiphase fluid flow in structurally complex reservoirs in Jolley, S.J., Barr, D., Walsh J.J., and Knipe R.J., eds., Structurally Complex Reservoirs: Geological Society of London Special Publication 292, p. 405–429.

McCabe, C., and Elmore, R.D., 1989, The occurrence and origin of Late Paleozoic remagnetization in the sedimentary rocks of North America: Reviews of Geophysics, v. 27, p. 471–494.

McLimans, R.K., Barnes, H.L., and Ohmoto, H., 1980, Sphalerite stratigraphy of the upper Mississippi valley lead-zinc district, southwest Wisconsin: ECONOMIC GEOLOGY, v. 75, p. 351–361.

Micklethwaite, S., Sheldon, H.A., and Baker, T., 2010, Active fault and shear processes and their implications for mineral deposit formation and discovery: Journal of Structural Geology, v. 32, p. 151–165.

Miller, S.A., Collettini, C., Chiaraluce, L., Cocco, M., Barchi, M., and Kaus, B.J.P., 2004, Aftershocks driven by a high-pressure CO$_2$ source at depth: Nature, v. 427, p. 724–727.

Misra, K.C., 2000, Understanding mineral deposits: Dordrecht, Netherlands, Kluwer, 845 p.

Morrow, C.A., Shi, L.Q., and Byerlee, J.D., 1984, Permeability of fault gouge under confining pressure and shear stress: Journal of Geophysical Research, v. 89, p. 3193–3200.

Neuzil, C.E., 1994, How permeable are clays and shales?: Water Resources Research, v. 30, p. 145–150.

——1995, Abnormal pressures as hydrodynamic phenomena: American Journal of Science, v. 295, p. 742–786.

——2003, Hydromechanical coupling in geologic processes: Hydrogeology Journal, v. 11, p. 41–83.

Nunn, J. A., and Lin, G., 2002, Insulating effect of coals and organic rich shales: Implications for topography-driven fluid flow, heat transport, and genesis of ore deposits in the Arkoma basin and Ozark plateau: Basin Research, v. 14, p. 129–145.

Ohtake, M., and Nakahara, H., 1999, Seasonality of great earthquake occurrence at the northwestern margin of the Philippine Sea Plate: Pure and Applied Geophysics, v. 155, p. 689–700.

Oliver, J., 1986, Fluids expelled tectonically from orogenic belts: Their role in hydrocarbon migration and other geologic phenomena: Geology, v. 14, p. 99–102.

Ortiz, N. V., Ferentchak, J. A., Ethridge, F. G., Granger, H. C., and Sunada, D. K., 1980, Ground-water flow and uranium in Colorado Plateau: Groundwater, v. 18, p. 596–606.

Paluszny, A., and Matthai, S.K., 2009, Numerical modeling of discrete multi-crack growth applied to pattern formation in geological brittle media: International Journal of Solids and Structures, v. 46, p. 3383–3397.

——2010, Impact of fracture development on the effective permeability of porous rocks as determined by 2-D discrete element fracture growth modeling: Journal of Geophysical Research, v. 115, B02203, doi:10.1029/2008JB006236.

Pan, H., Symons, D.T.A., and Sangster, D.F., 1990, Paleomagnetism of the Mississippi Valley-type ores in the northern Arkansas and Tri-State districts: ECONOMIC GEOLOGY, v. 27, p. 923–931.

Parry, W.T., Hedderly-Smith, D., and Bruhn, R.L., 1991, Fluid inclusions and hydrothermal alteration on the Dixie Valley fault, Nevada: Journal of Geophysical Research, v. 96, p. 19,733–19,748.

Peacock, S.M., 1989, Numerical constraints on rates of metamorphism, fluid production, and fluid flux during regional metamorphism: Geological Society of America Bulletin, v. 101, p. 476–485.

Pelch, M.A., 2011, Composition of fluid inclusions from the Cave-in-Rock bedded-replacement fluorite deposits in the Illinois-Kentucky district: Unpublished M.S. thesis, University of Missouri, Columbia, 52 p.

Phillips, O.M., 2009, Geological fluid dynamics—sub-surface flow and reactions: Cambridge, UK, Cambridge University Press, 285 p.

Piqué, À., Canals, À., Grandia, F., and Banks, D.A., 2008, Mesozoic fluorite veins in NE Spain record regional base metal-rich brine circulation through basin and basement during extensional events: Chemical Geology, v. 257, p. 139–152.

Plumlee, G.S., 1989, Processes controlling epithermal mineral distribution in the Creede mining district, Colorado: Unpublished Ph.D. thesis, Cambridge, Massachusetts, Harvard University, 389 p.

Pokrovski, G.S., Tagirov, B.R., Schott, J., Hazemann, J.-L., and Proux, O., 2009, A new view on gold speciation in sulfur-bearing hydrothermal fluids from in situ X-ray absorbtion spectroscopy and quantum-chemical modeling: Geochimica et Cosmochimica Acta, v. 73, p. 5406–5427.

Pruess, K., 1991, TOUGH2—a general-purpose numerical simulator for multiphase fluid and heat flow: Berkeley, CA, Lawrence Berkeley National Laboratory Report LBL-29400.

Pruess, K., Oldenburg, C., and Moridis, G., 1999, TOUGH2 user's guide, version 2.0: Berkeley, CA, Lawrence Berkeley National Laboratory Report LBNL-43134.

Ragan, V.M., Coveney, R.M., Jr., and Brannon, J.C., 1996, Migration paths for fluids and northern limits of the Tri-State district from fluid inclusions and radiogenic isotopes: Society of Economic Geologists Special Publication 4, p. 419–431.

Rahman, M.K., Hossain, M.M., and Rahman, S.S., 2002, A shear-dilation-based model for evaluation of hydraulically stimulated naturally fractured reservoirs: International Journal for Numerical and Analytical Methods in Geomechanics, v. 26, p. 469–497.

Raleigh, C.B., Healy, J.H., and Bredehoeft, J.D., 1976, An experiment in earthquake control at Rangely, Colorado: Science, v. 191, p. 1230–1236.

Redmond, P.B., Einaudi, M.T., Inan, E.E., Landtwing, M.R., and Heinrich, C.A., 2004, Copper deposition by fluid cooling in intrusion-centered systems: New insights from the Bingham porphyry ore deposit, Utah: Geology, v. 32, p. 217–220.

Reed, M., and Palandri, J., 2010, Ascent and cooling of magmatic fluids: Precipitation of vein and alteration minerals, *in* Birkle, P., and Torres-Alvarado, I., eds., Water-rock interaction XIII: London, Taylor and Francis, p. 37–40.

Reed, M., and Spycher, N., 1984, Calculation of pH and mineral equilibria in hydrothermal waters with application to geothermometry and studies of boiling and dilution: Geochimica et Cosmochimica Acta, v. 48, p. 1479–1492.

Rice, J.R., 1992, Fault stress states, pore pressure distributions, and the weakness of the San Andreas fault, *in* Evans, B., and Wong, T.-F., eds., Fault mechanics and transport properties of rocks: San Diego, CA, Academic Press, p. 475–503.

Richards, J.P., and Tosdal, R.M., 2001, Preface: Reviews in Economic Geology, v. 14, p. vi.

Rojstaczer, S.A., Ingebritsen, S.E., and Hayba, D.O., 2008, Permeability of continental crust influenced by internal and external forcing: Geofluids, v. 8, p. 128–139.

Rojstaczer, S.A., Wolf, S., and Michel, R., 1995, Permeability enhancement in the shallow crust as a cause of earthquake-induced hydrological changes: Nature, v. 373, p. 237–239.

Rowan, E.L., 1986, Cathodoluminescent zonation in hydrothermal dolomite cements: Relationship to Mississippi Valley-type Pb-Zn mineralization in southern Missouri and northern Arkansas, *in* Hagni, R. D., ed., Proceedings Process Mineralogy. VI: Including applications to precious metals and cathodoluminescence: New Orleans, American Institute of Mining Engineers, p. 69–87.

Ruff, L.J., 2004, Limits of the seismogenic zone, *in* Karner, G.D., Taylor, B., Driscoll, N.W., Kohlstedt, D. L., eds., Rheology and deformation of the lithosphere at continental margins: New York, Columbia University Press, p. 138–165.

Rusk, B.G., Reed, M.H., Dilles, J.H., Klemm, L.M., and Heinrich, C.A., 2004, Compositions of magmatic fluids determined by LA-ICP-MS of fluid inclusions from the porphyry copper-molybdenum deposit at Butte, MT: Chemical Geology, v. 210, p. 173–199.

Rusk, B.G., Reed, M.H., and Dilles, J.H., 2008, Fluid inclusion evidence for magmatic-hydrothermal fluid evolution in the porphyry copper-molybdenum deposit at Butte, Montana: ECONOMIC GEOLOGY, v. 103, p. 307–334.

Russell, M.J., 1978, Downward-excavating hydrothermal cells and Irish type ore deposits: Importance of an underlying thick Caledonian prism: Institution of Mining and Metallurgy Transactions, v. 87, p. B168–B171.

Rutqvist, J., Wu, Y.S., Tsang, C.F., and Bodvarsson, G., 2002, A modeling approach for analysis of coupled multiphase fluid flow, heat transfer, and deformation in fractured porous rock: International Journal of Rock Mechanics and. Mineral Science, v. 39, p. 429–442.

Saar, M.O., and Manga, M., 2004, Depth dependence of permeability in the Oregon Cascades inferred from hydrogeologic, thermal, seismic, and magmatic modeling constraints: Journal of Geophysical Research, v. 109, doi:10.1029/2003JB002855.

Sanford, R.F., 1990, Hydrogeology of an ancient arid closed basin: Implications for tabular sandstone-hosted uranium deposits: Geology, v. 18, p. 1099–1102.

——1992, A new model for tabular-type uranium deposits: ECONOMIC GEOLOGY, v. 87, p. 2041–2055.

——1994, A quantitative model of ground-water flow during formation of tabular sandstone uranium deposits: ECONOMIC GEOLOGY, v. 89, p. 341–360.

Sass, J.H., Lachenbruch, A.H., Moses, T.H., Jr., and Morgan, P., 1992, Heat flow from a scientific research well at Cajon Pass, California: Journal of Geophysical Research v. 97, p. 5017–5030.

Sato, T., Sakai, R., Furuya, K., and Kodama, T., 2000, Coseismic spring flow changes associated with the 1995 Kobe earthquake: Geophysical Research Letters, v. 27, p. 1219–1222.

Savage, M.K., 2010, The role of fluids in earthquake generation in the 2009 $M_w$6.3 L'Aquila, Italy earthquake and its foreshocks: Geology, v. 38, p. 1055–1056.

Schulze-Makuch, D., 2005, Longitudinal dispersivity data and implications for scaling behavior: Ground Water, v. 43, p. 443–456.

Schwartz, F.W., and Zhang, H., 2003, Fundamentals of groundwater: New York, Wiley and Sons, 583 p.

Seyfried, W.E., Jr., 1987, Experimental and theoretical constraints on hydrothermal alteration processes at mid- ocean ridges: Annual Review of Earth and Planetary Sciences, v. 15, p. 317–335.

Sharp, J.M., Jr., 1978, Energy and momentum transport model of the Ouachita basin and its possible impact on formation of economic mineral deposits: ECONOMIC GEOLOGY, v. 73, p. 1057–1068.

Shinohara, H., 2008, Excess degassing from volcanoes and its role on eruptive and intrusive activity: Reviews of Geophysics, v. 46, doi:10.1029/2007RG000244.

Shinohara, H., and Hedenquist, J.W., 1997, Constraints on magma degassing beneath the Far Southeast porphyry Cu-Au deposit, Philippines: Journal of Petrology, v. 38, p. 1741–1752.

Shmonov, V.M., Vitiovtova, V.M., Zharikov, A.V., and Grafchikov, A.A., 2002, Fluid permeability of the continental crust: Estimation from experimental data: Geochemistry International, v. 40, Suppl. 1, p. S3–S13.

——2003, Permeability of the continental crust: Implications of experimental data: Journal of Geochemical Exploration, v. 78–79, p. 697–699.

Sibson, R.H., 1987, Earthquake rupturing as a hydrothermal mineralizing agent: Geology, v. 15, p. 704–707.

——2001, Seismogenic framework for hydrothermal transport and ore deposition: Reviews in Economic Geology, v. 14, p. 25–50.

Sibson, R.H., and Rowland, J.V., 2003, Stress, fluid pressure, and structural permeability in seismogenic crust, North Island, New Zealand: Geophysical Journal International, v. 154, p. 584–594.

Sibson, R.H., Moore, J.M.M., and Rankin, A.H., 1975, Seismic pumping—a hydrothermal fluid transport mechanism: Journal of the Geological Society of London, v. 131, p. 653–659.

Sibson, R.H., Robert, F., and Poulsen, K.H., 1988, High-angle reverse faults, fluid-pressure cycling, and mesothermal gold-quartz deposits: Geology, v. 16, p. 551–555.

Sillitoe, R.H., 2005, Supergene oxidized and enriched porphyry copper and related deposits: ECONOMIC GEOLOGY 100TH ANNIVERSARY VOLUME, p. 723–768.

Sillitoe, R.H., and Meinert, L.D., 2010, Porphyry copper systems: ECONOMIC GEOLOGY, v. 105, p. 3–41.

Simmons, S.F., and Brown, K.L., 2006, Gold in magmatic hydrothermal solutions and the rapid formation of a giant ore deposit: Science, v. 314, p. 288–291.

Simmons, S.F., White, N.C., and John, D.A., 2005, Geological characteristics of epithermal precious and base metal deposits: ECONOMIC GEOLOGY 100TH ANNIVERSARY VOLUME, p. 455–522.

Snow, D.T., 1968, Rock fracture spacings, openings, and porosities: Proceedings American Society of Civil Engineers, v. 94, p. 73–91.

Stober, I., and Bucher, K., 2007, Hydraulic properties of the crystalline basement: Hydrogeology Journal, v. 15, p. 213–224.

Stoffell, B., Appold, M.S., Wilkinson, J.J., McClean, N.A., and Jeffries, T.E., 2008, Geochemistry and evolution of Mississippi Valley-type mineralizing brines from the Tri-State and northern Arkansas districts determined by LA-ICP-MS microanalysis of fluid inclusions: ECONOMIC GEOLOGY, v. 103, p. 1411–1435.

Streit, J.E., and Cox, S.F., 1998, Fluid infiltration and volume change during mid-crustal mylonitization of Proterozoic granite, King Island, Tasmania: Journal of Metamorphic Geology, v. 16, p. 197–212.

Symonds, R.B., Gerlach, T.M., and Reed, M.H., 2001, Magmatic gas scrubbing: Implications for volcano monitoring: Journal of Volcanology and Geothermal Research, v. 108, p. 303–341.

Symons, D.T A., and Sangster, D.F., 1991, Paleomagnetic age of the central Missouri barite deposits and its genetic significance: ECONOMIC GEOLOGY, v. 86, p. 1–12.

Symons, D.T.A., Pannalal, S.J., Coveney, R.M., Jr., and Sangster, D.F., 2005, Paleomagnetism of late Paleozoic strata and mineralization in the Tri-State lead-zinc ore district: ECONOMIC GEOLOGY, v. 100, p. 295–309.

Talwani, P., Chen, L., and Gahalaut, K., 2007, Seismogenic permeability, $k_s$: Journal of Geophysical Research, v. 112, doi:10.1029/2006JB004665.

Taylor, H.P., Jr., 1979, Oxygen and hydrogen isotope relationships in hydrothermal mineral deposits, *in* Barnes, H.L., ed., Geochemistry of hydrothermal ore deposits: New York, John Wiley and Sons, p. 173–235.

Terakawa, T., Zoporowski, A., Galvan, B., and Miller, S.A., 2010., High-pressure fluid at hypocentral depths in the L'Aquila region inferred from earthquake focal mechanisms: Geology, v. 38, p. 995–998.

Thomas, B.E., 1989, Simulation analysis of the ground-water system in Mesozoic rocks in the Four Corners area, Utah, Colorado, Arizona, and New Mexico: U.S. Geological Survey Water-Resources Investigations Report 88-4086, 89 p.

Titley, S.R., 1978, Geologic history, hypogene features, and processes of secondary sulfide enrichment at the Pleysumi copper prospect, New Britain, Papua New Guinea: ECONOMIC GEOLOGY, v. 73, p. 768–784.

——1990, Evolution and style of fracture permeability in intrusion-centered hydrothermal systems, *in* Bredehoeft, J.D., and Norton, D.L., eds., The role of fluids in crustal processes: Washington, D.C., National Academy Press, p. 50–63.

Tóth, J., 1963, A theoretical analysis of groundwater flow in small drainage basins: Journal of Geophysical Research, v. 68, p. 4795–4812.

Townend, J., and Zoback, M.D., 2000, How faulting keeps the crust strong: Geology, v. 28, p. 399–402.

Turner-Peterson, C.E., and Hodges, C.A., 1986, Descriptive model of sandstone U: U.S. Geological Survey Bulletin 1693, p. 209–210.

U.S. Bureau of Reclamation, 2001, Engineering geology field manual, 2nd ed.: v. II, p. 107–182.

U.S. Geological Survey, 2011, Metals and mMinerals: U.S. Geological Survey Minerals Yearbook 2009, v. I, p. 42.1–42.2.

Vineyard, J.D., 1977, Preface to the Viburnum Trend issue: ECONOMIC GEOLOGY, v. 72, p. 337–338.

Von Damm, K. L., 1990, Seafloor hydrothermal activity: Black smoker chemistry and chimneys: Annual Review of Earth and Planetary Sciences, v. 18, p. 173–204.

——1995, Controls on the chemistry and temporal variability of seafloor hydrothermal: American Geophysical Union Geophysical Monograph 91, p. 222–247.

Walder, J., and Nur, A., 1984, Porosity reduction and crustal pore pressure development: Journal of Geophysical Research, v. 89, p. 11,539–11,548.

Wang, C.-Y., and Manga, M., 2010, Earthquakes and water: Berlin-Heidelberg, Germany, Springer-Verlag, 227 p.

Wang, H.F., 2000, Theory of linear poroelasticity with applications to geomechanics and hydrogeology: Princeton, NJ, Princeton University Press, 287 p.

Wenz, Z.J., Appold, M.S., Shelton, K.L., and Tesfaye, S., 2012, Geochemistry of Mississippi Valley-type mineralizing fluids of the Ozark Plateau: A regional synthesis: American Journal of Science, v. 312, p. 22–80.

Wilkinson, J.J., Everett, C.E., Boyce, A.J., Gleeson, S.A., and Rye, D.M., 2005, Intracratonic crustal seawater circulation and the genesis of subseafloor zinc-lead mineralization in the Irish orefield: Geology, v. 33, p. 805–808.

Wilkinson, J.J., Stoffell, B., Wilkinson, C.C., Jeffries, T.E., and Appold, M. S., 2009, Anomalously metal-rich fluids from hydrothermal ore deposits: Science, v. 323, p. 764–767.

Willis, G.F., and Tosdal, R.M., 1992, Formation of gold veins and breccias during dextral strike-slip faulting in the Mesquite mining district, southeastern California: ECONOMIC GEOLOGY, v. 87, p. 2002–2022.

Willis-Richards, J., Watanabe, K., and Takahashi, H., 1996, Progress towards a stochastic rock mechanics model of engineered geothermal systems: Journal of Geophysical Research, v. 101, p. 17,481–17,496.

Wisniowiecki, M. J., Van der Voo, R., McCabe, C., and Kelly, W. C., 1983, A Pennsylvanian paleomagnetic pole from the mineralized late Cambrian Bonneterre Formation, Southeast Missouri: Journal of Geophysical Research, v. 88, p. 6540-6548.

Wolf, L.W., Rowe, C.A., and Horner, R.B., 1997, Periodic seismicity on the Alaska-British Columbia border: A case for hydrologically triggered earthquakes: Bulletin of the Seismological Society of America, v. 87, p. 1473–1483.

Wu, Y., and Beales, F., 1981, A reconnaissance study by paleomagnetic methods of the age of mineralization along the Viburnum Trend, Southeast Missouri: ECONOMIC GEOLOGY, v. 76, p. 1879–1894.

Xu, T., Sonnenthal, E., Spycher, N. and Pruess, K., 2004, TOUGHREACT user's guide: A simulation program for non-isothermal multiphase reactive geochemical transport in variable saturated geologic media: Berkeley, CA, Lawrence Berkeley National Laboratory Paper LBNL-55460.

Yardley, B.W.D., 1986, Fluid migration and veining in the Connemara Schists, *in* Walther, J.V., and Wood, B.J., eds., Fluid-rock reactions during metamorphism: Advances in Physical Geochemistry, v. 5, New York, Springer-Verlag, p. 109–131.

Yardley, B.W.D., and Baumgartner, L.P., 2007, Fluid processes in deep crustal fault zones, *in* Handy, M.R., Hirth, G., and Hovius, N., eds., Tectonic faults—agents of change on a dynamic earth: Cambridge, Massachusetts, MIT Press, p. 295–318.

Zhao, C., Hobbs, B.E., and Mulhaus, H.B., 1998, Finite element modelling of temperature gradient driven rock alteration and mineralization in porous rock masses: Computer Methods in Applied Mathematics and Engineering, v. 165, p. 175–187.

Zielinsky, R.A., 1982, The mobility of uranium and others elements during alteration of rhyolitic ash to montmorillonite: A case study in the Troublesome Formation, Colorado, U.S.A.: Chemical Geology, v. 35, p. 185–204.

Zyvoloski, G.A., Dash, Z.V., and Kelkar, S., 1988, FEHM: Finite element heat and mass transfer code: Los Alamos, NM, Los Alamos National Laboratory Report LA-11224-MS.

Zyvoloski, G.A., Robinson, B.A., Dash, Z.D., and Trease, L.L., 1997, Summary of models and methods for the FEHM application—a finite-element heat- and mass-transfer code: Los Alamos, NM, Los Alamos National Laboratory Report LA-13307MS.

## APPENDIX

Notation

$a$ = total fracture aperture after dilation
$a_0$ = initial aperture
$A$ = cross sectional area [$L^2$]
$b$ = thickness [L]
$c$ = specific heat capacity (usually isobaric heat capacity) [$E\,M^{-1}\,T^{-1}$]
$c_b$ = bulk compressibility of porous medium at constant fluid pressure [$L\,t^2\,M^{-1}$]
$c_s$ = bulk compressibility of rock matrix [$L\,t^2\,M^{-1}$]
$c_u$ = uniaxial compressibility of the porous medium [$L\,t^2\,M^{-1}$]
$C$ = aqueous concentration [$M\,L^{-3}$]
$D$ = hydrodynamic dispersion [$L^2\,t^{-1}$]
$D_w$ = diffusion coefficient in open water [$L^2\,t^{-1}$]
$E$ = energy [E]
$F$ = fluxibility [$M\,L^{-3}\,t^{-1}$]
$g$ = gravitational acceleration [$L\,t^{-2}$]
$G$ = shear modulus, [$M\,L^{-1}\,t^{-2}$].
$H$ = specific enthalpy [$E\,M^{-1}$]
$k$ = intrinsic permeability [$L^2$]
$k_0$ = reference intrinsic permeability [$L^2$]
$k_r$ = relative permeability [dimensionless]
$K$ = thermal conductivity [$E\,t^{-1}\,L^{-1}\,T^{-1}$]
$L$ = characteristic length or distance [L]
$M$ = mass [M]
$P$ = pressure [$M\,L^{-1}\,t^{-2}$]
$P_c$ = capillary pressure [$M\,L^{-1}\,t^{-2}$]
$\mathbf{q}$ = volumetric flow rate per unit area (volume flux, specific discharge or Darcy velocity) [$L\,t^{-1}$]
$R$ = general source/sink term for mass, heat, or chemical reactions [variable]
$s_s$ = specific storage [$L^{-1}$]
$S$ = volumetric saturation [$L^3\,L^{-3}$, dimensionless]
$t$ = time [t]
$T$ = temperature [T]
$\mathbf{u}$ = displacement vector [L]

$U_s$ = shear displacement [L]
$\mathbf{v}$ = average linear velocity (seepage velocity) [$L\,t^{-1}$]
$X$ = mass fraction $H_2O$, NaCl, or $CO_2$ in an $H_2O$-NaCl-$CO_2$ mixture [dimensionless]
$z$ = elevation above a datum, vertical Cartesian coordinate, or depth [L]
$z_g$ = elevation parallel to the direction of gravity [L]
$\alpha$ = dispersivity [L]
$\alpha_e$ = effective stress coefficient, [dimensionless]
$\alpha_T$ = porous medium linear thermal expansivity [$T^{-1}$]
$\beta$ = bulk fluid compressibility [$L\,t^2\,M^{-1}$]
$\theta$ = potential per unit mass [$E\,M^{-1}$]
$\lambda$ = coefficient of friction [dimensionless]
$\mu$ = dynamic viscosity [$M\,L^{-1}\,t^{-1}$]
$v$ = Poisson's ratio [dimensionless]
$\rho$ = density [$M\,L^{-3}$]
$\sigma$ = stress [$M\,L^{-1}T^{-2}$]
$\sigma_{eff}$ = effective normal stress
$\sigma_{nref}$ = effective normal stress to a fracture
$\tau$ = tortuosity [dimensionless]
$\phi$ = porosity [dimensionless]
$\phi_e$ = effective porosity [dimensionless]
$\Phi_{dil}$ = shear dilation angle
(^) indicates increase or decrease in a quantity
(-) indicates a nondimensionalized quantity

*Subscripts*

Unless otherwise locally redefined, subscripts have the following meanings:

f   refers to the fluid mixture in place (either a single phase or a two-phase mixture)
l   refers to liquid
m   refers to the porous medium
r   refers to the rock
v   refers to vapor (steam)
0   refers to an initial state